Diploma thesis

Histogram analysis of lung CT scans of pulmonary hypertension patients

submitted by

Martin Wurm

Date of birth: 9th March, 1988

for the Academic Degree of

Doktor der gesamten Heilkunde

(Dr. med. univ.)

Medical University of Graz

Ludwig Boltzmann Institute for Lung Vascular Research

Thesis supervisors: Univ. Prof. DDr. Andrea Olschewski

Dr. Zoltán Bálint, DI Michael Pienn

Graz, 13th May 2014 Martin Wurm

Statutuory declaration

I declare that I have authored this thesis independently, that I have not used other than the declared sources / resources, and that I have explicitly marked all material which has been quoted either literally or by content from the used sources.

Graz, 13th May 2014 *Martin Wurm*

Acknowledgements

I would like to thank the members of the Ludwig Boltzmann Institute for Lung Vascular Research for all the help and advice they gave to me. The ongoing discussions provided valuable improvements and this work would not have been possible without you. Furthermore, I want to thank Univ. Prof. DDr. Andrea Olschewski and Univ. Prof. Dr. Horst Olschewski for giving me the chance to write my diploma thesis at the LBI and for all the clinical knowledge I was able to learn from you. Also I want to thank Dr. Zoltán Bálint and DI Michael Pienn for introducing me to scientific work and for all the interesting and fun moments I shared with you.

This work would not have been possible without the help of my family, who supported me in every way one could imagine and Judith and Noah, to both I dedicate all the motivation and encouragement.

Abstract

The evaluation of the X-ray attenuation in the lung parenchyma by histogram analysis can give relevant information to quantify pathologic changes in the lung. The main goal of this thesis is to develop an algorithm for lung CT image analysis and to identify diagnostically relevant parameters for pulmonary hypertension (PH) and associated lung diseases, via correlation with patient clinical data. In a clinical CT study of 25 patients we retrospectively applied an automated algorithm to provide statistical information of the lung parenchyma of them. Quantitative readouts of lung parenchyma histograms of patients with and without PH were computed. Statistical analysis has been performed of Hounsfield units and lung perfused blood volume and histograms, skewness, kurtosis, full-width at half-maximum and normalized peak height have been compared. We found specific quantitative parameters of perfused blood volume histograms to differentiate between PH and non-PH patients in our patient cohort.

Kurzfassung

Die Analyse von Histogrammen erstellt aus Computertomographie-Schnittbildern kann wertvolle Anhaltspunkte für pathologische Veränderungen der Lunge liefern. Relevante Informationen im Hinblick auf Lungenhochdruck und ähnlichen Lungenerkrankungen sollten mit den klinischen Daten des Patienten in Verbindung gebracht werden. Es wurde eine Pilotstudie an der 25 Patienten teilnahmen durchgeführt und die Lungenparenchyminformation retrospektiv analysiert und statistisch ausgewertet. Die Lungengefäße wurden isoliert um einen unabhängigen Vergleich zwischen Parenchym, Gefäßen und der gesamten Lunge zu ermöglichen. Die statistische Analyse wurde von Hounsfield units und perfundiertem Lungenblutvolumen durchgeführt, wobei Histogramm, Schiefe, Wölbung, Halbwertsbreite und normalisiertes Maximum von Patienten mit und ohne Lungenhochdruck errechnet wurden. Durch unsere Arbeit konnten wir verschiedene Indikatoren für Lungenhochdruck feststellen. Verschiedene Parameter der Histogrammanalyse von Lungenperfusions-Blutvolumen ermöglichten in unserer Patientenkohorte die Unterscheidung zwischen Lungenhochdruck-Patienten und Patienten ohne Lungenhochdruck.

Contents

1 Introduction **13**

1.1 General hypothesis 13

1.2 Pulmonary hypertension (PH) 13

1.2.1 Definition 13

1.2.2 WHO classification 14

1.2.3 Pathology of pulmonary hypertension 16

1.2.3.1 Pulmonary arterial hypertension (PAH) and pulmonary veno-occlusive disease (PVOD) 16

1.2.3.2 Pulmonary hypertension owing to left heart disease 17

1.2.3.3 Pulmonary hypertension owing to lung diseases and / or hypoxia 17

1.2.3.4 Chronic thromboembolic pulmonary hypertension (CTEPH) 18

1.2.3.5 Pulmonary hypertension with unclear multifactorial mechanisms 19

1.2.4 Time to diagnosis and outcome 19

1.2.5 Treatment of PH 19

1.2.6 Non-invasive diagnosis of PH 20

1.3 Computed tomography (CT) 21

1.3.1 CT for clinical PH diagnosis 21

1.3.2 Dual-energy computed tomography (DECT) 23

1.4 Objectives 23

2 Materials and Methods **24**

2.1 Patient population 24

2.2 Computed tomography (CT) 24

2.3 Right heart catheterization (RHC) 24

2.4 Lung Perfused Blood Volume 25

2.5 Histogram analysis 25

2.6 3D-segmentation of lung parenchyma 26

2.6.1 Denoising of the CT images and HU analysis 26

2.6.2 Key steps in getting an accurate segmentation 26

2.6.3 Isolation of the trachea and exclusion of vessels 27

2.6.4 Gradient calculation to sharpen the edges of lung parenchyma 27

2.6.5 Post-processing of the CT images 28

2.7 Quantitative analysis of the CT-scan data 29

2.7.1 Histogram 29

2.7.2 Mean lung attenuation (MLA) 30
2.7.3 Skewness 30
2.7.4 Kurtosis 30
2.7.5 Full-width at half-maximum (FWHM) 31
2.7.6 Normalized peak height (N_peak) 31
2.7.7 Statistical analysis 32

3 Results **33**
3.1 Patient characteristics 33
3.1.1 Associated diseases 34
3.1.2 Bolus timing 35
3.2 Lung Segmentation 36
3.2.1 Advantages 36
3.2.2 Disadvantages 36
3.2.3 Quality control of segmentation 37
3.3 HU histogram analysis 37
3.3.1 Correlations with HU histogram data 38
3.3.2 Correlation with image noise 43
3.4 LungPBV histogram analysis 45
3.4.1 Correlations with LungPBV data 46
3.4.2 Correlations of LungPBV data with image noise 48
3.4.3 Difference between quantitative parameters and WHO class 48
3.4.4 Differentiation between PH and non-PH patients 50

4 Discussion **52**
4.1 Limitations 53
4.2 Outlook 53
4.3 Conclusion 54

5 Bibliography **55**

List of Abbreviations

ALK-1	activin-receptor-like kinase
ANA	anti-nuclear antibodies
art SO2	arterial oxygen saturation
BMPR2	bone morphogenetic protein receptor 2
BSA	body surface area
CHD	congenital heart disease
CMR	cardiac magnetic resonance
CO	cardiac output
COPD	chronic obstructive pulmonary disease
CT	computed tomography
CTD	connective tissue disease
CTEPH	chronic thromboembolic pulmonary hypertension
DECT	dual energy computed tomography
FWHM	full-width at half-maximum
HHT	hereditary haemorrhagic telangiectasia
HRCT	high-resolution computed tomography
HU	Hounsfield Units
ILD	interstitial lung disease
IPF	idiopathic pulmonary fibrosis
LBI	Ludwig Boltzmann Institute
LBI LVR	Ludwig Boltzmann Institute for Lung Vascular Research
LFT	liver function test
MLA	mean lung attenuation
mPAP	mean pulmonary arterial pressure
PBV	perfused blood volume
PCH	pulmonary capillary hemangiomatosis
PFT	pulmonary function test
PH	Pulmonary hypertension
Ppa	mean pulmonary arterial pressure
Ppcw	pulmonary capillary wedge pressure
PVOD	pulmonary veno-occlusive disease
PVR	pulmonary vascular resistance
RCT	randomized controlled trial
RHC	right heart catheterization
SVR	systemic vascular resistance
TEE	transoesophageal echocardiagraphy
TLC	total lung capacity
US	ultrasonography
V'/Q'	ventilation / perfusion lung scan
ven SO2	venous oxygen saturation
WHO	world health organization

List of Figures

1.1 Colored lung vasculature and airways (red = arteries, blue = veins)[65]. 14
1.2 Muscularized pulmonary artery from an IPAH patient[16]. 16
1.3 Representative CT scan of a patient from our PH pilot study, suspect of PH caused by left heart disease. 17
1.4 CT scan showing the lung of a patient from our PH pilot study with idiopathic pulmonary fibrosis (IPF). 18
1.5 DE-CT scan with overlay of denoised iodine perfusion CT scan of a patient from our PH pilot study with suspect CTEPH. 18
1.6 Evidence-based treatment algorithm for patients with pulmonary arterial hypertension (for group 1 patients only)[21]. 20
1.7 A representative CT scan of a patient from our PH pilot study showing the aorta (Ao) and the dilated main pulmonary artery (PA). 21
1.8 Diagnostic Approach to Pulmonary Hypertension. BGA = blood gas analysis, CHD = congenital heart disease, CTD = connective tissue disease, CTEPH = chronic thromboembolic pulmonary hypertension, DLCO = diffusion capacity of the lung for carbon monoxide, ECG = electrocardiogram, HR-CT = high-resolution computed tomography, PA = pulmonary angiography, PAH = pulmonary arterial hypertension, PAPm = mean pulmonary arterial pressure, PAWP = pulmonary arterial wedge pressure, PCH = pulmonary capillary hemangiomatosis, PEA = pulmonary endarterectomy, PFT = pulmonary function testing, PH = pulmonary hypertension, PVOD = pulmonary veno-occlusive disease, PVR = pulmonary vascular resistance, RHC = right heart catheter, RV = right ventricle, V/Q = ventilation/perfusion, x-ray = chest radiograph[30]. 22

2.1 A representative LungPBV scan of a patient from the PH pilot study with CTEPH after pulmonary endarterectomy 25
2.2 Image processing procedures: Dilation and Erosion[64]. 27
2.3 Left: 3D array of all CT images of a representative CT scan, segmented by 3D balls of different sizes shown as green on the picture. Right: Lung parenchyma segmentation viewed in 3D. 27
2.4 CT scan image of a patient, (left) original image, (right) image after segmentation of lung parenchyma. Color coding: dark green = right lung, light green = left lung. 28

2.5 A: Representative CT image of a patient from our PH pilot study. B: Histogram of the whole CT scan of the corresponding patient. C: Representative CT image of a patient of our PH pilot study. D: Histogram of the whole CT scan of the corresponding patient. 29
2.6 Left: Skewness of a representative Hounsfield unit based CT histogram by image number. Right: Kurtosis of a histogram by image number 31
2.7 Left: Full-width at half-maximum of a histogram. The FWHM is delineated by the left and right dark and light green dashed lines, respectively. Right: Normalized peak height of a histogram. 32

3.1 3D segmentation of the right lung (orange) and the left lung (yellow) from a representative patient from our PH pilot study 36
3.2 Correlations of HU histogram data with art SO_2. 40
3.3 Correlations of HU histogram data with TLC. 42
3.4 Correlations of HU histogram data with image noise of air 44
3.5 Correlations of LungPBV data with art SO_2 47
3.6 WHO class, LungPBV FWHM and normalized peak height. Center lines indicate the mean, whiskers represent the standard deviation. (* $p < 0.05$) 49
3.7 Differentiation between PH and non-PH patients. avgΔAttenuation = average attenuation difference, PH = pulmonary hypertension. (* $p < 0.05$) 50
3.8 Values of other histogram parameters. 51

List of Tables

1.1 Updated Clinical Classification of Pulmonary Hypertension (Nice 2013). BMPR = bone morphogenic protein receptor type II; CAV1 = caveolin-1; ENG = endoglin; HIV = human immunodeficiency virus; PAH = pulmonary arterial hypertension[54]. 15

3.1 Patient characteristics (BSA = body surface area, mPAP = mean pulmonary arterial pressure, PAWP = pulmonary artery wedge pressure, CO = cardiac output, PVR = pulmonary vascular resistance, $AVDO_2$ = arteriovenous oxygen difference, $artSO_2$ = arterial oxygen saturation, $venSO_2$ = venous oxygen saturation). 33

3.2 Associated diseases of all patients in the clinical PH pilot study (PH = pulmonary hypertension, IPAH = idiopathic pulmonary arterial hypertension, PEA = pulmonary endarterectomy, ILD = interstitial lung disease, OSAS = obstructive sleep apnoea syndrome). 34

3.3 Bolus timing (PA = pulmonary artery, LA = left atrium). 35

3.4 HU histogram data of all histogram parameters previously described. STD = standard deviation, Skew = skewness, Kurt = kurtosis, FWHM = full-width at half-maximum, N_peak = normalized peak. 37

3.5 HU histogram Spearman correlations with RHC parameters, left lung. 38

3.6 HU histogram Spearman correlations with RHC parameters, right lung. 38

3.7 HU histogram data linear regression with lung function parameters. 41

3.8 HU histogram Spearman correlation with noise in air and noise in fat. 43

3.9 LungPBV data of all histogram parameters previously described. STD = standard deviation, Skew = skewness, Kurt = kurtosis, FWHM = full-width at half-maximum, N_peak = normalized peak. 45

3.10 LungPBV Spearman correlations with RHC parameters, left lung (avgΔAtt = average change in attenuation). 46

3.11 LungPBV Spearman correlations with RHC parameters, right lung (avgΔAtt = average change in attenuation). 46

3.12 Spearman correlations of LungPBV data with image noise. 48

Chapter 1

Introduction

1.1 General hypothesis

The aim of this study was to improve the diagnostic value of computed tomography (CT) of pulmonary hypertension patients. By means of quantitative analysis of lung CT histograms we aimed to provide relevant diagnostic data for non-invasive detection of lung diseases, especially pulmonary hypertension (PH). Furthermore, without increasing radiation dose for a patient, we wanted to specify signs of pulmonary hypertension. To achieve this goal, we attempted to create an automated algorithm with minimal user intervention for lung CT scan analysis.

1.2 Pulmonary hypertension (PH)

1.2.1 Definition

Pulmonary hypertension (PH) is a severe chronic disease of the lung vasculature and is defined as a mean pulmonary arterial pressure (mPAP) greater than 25 mmHg at rest[30]. There are numerous causes for PH and the pathophysiologic background of most subtypes is not clarified yet. Factors like age and body mass index can also affect mPAP. Healthy patients show mPAP values of 14.0±3.3 mmHg[36], but always below 20 mmHg. Older patients with an increased body mass index often present higher mPAP values, but still below 25 mmHg[46]. The gold standard for diagnosis is the right heart catheterization (RHC), an invasive procedure where the mPAP is measured directly using a probe in the right ventricle and the lung arteries[18]. Resting mPAP of 17 mmHg and above can also lead to reduced survival and adverse events if other diseases are present. This has been shown in several studies on chronic obstructive pulmonary disease (COPD) and lung fibrosis patients[24, 34, 61]. Recent literature also states that although a patients resting mPAP is in a healthy range, exceeding exercise pressure levels can occur[35]. Borderline pulmonary arterial pressure can therefore be a sign for pulmonary vasculopathy. Additionally, other diseases like intrathoracic pressure elevation and left ventricular impairment are a possible cause of this disease[60].

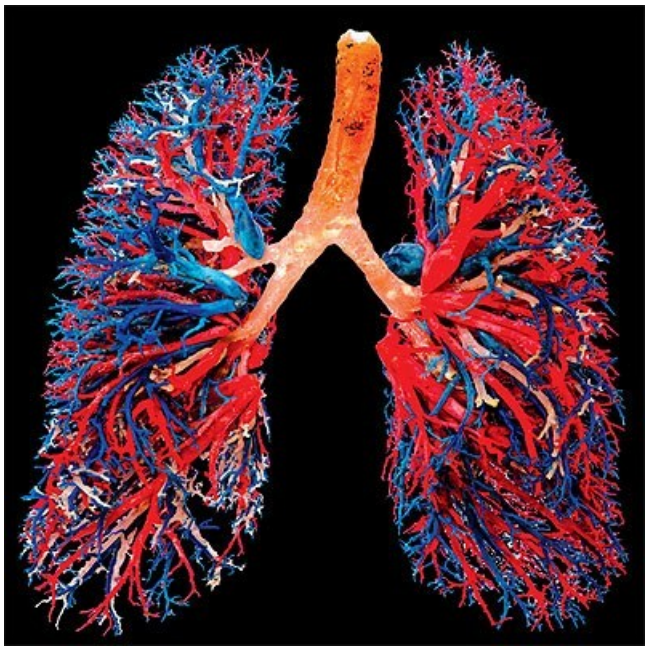

Figure 1.1 – Colored lung vasculature and airways (red = arteries, blue = veins)[65].

1.2.2 WHO classification

According to the most recent WHO classification on pulmonary hypertension from Nice 2013 (5th World Symposium), France, PH is divided to five subgroups[54]:

1. Pulmonary Arterial Hypertension (PAH)

   1'. Pulmonary veno-occlusive disease (PVOD) and / or pulmonary capillary hemangiomatosis (PCH)

   1". Persistent pulmonary hypertension of the newborn (PPHN)

2. Pulmonary hypertension owing to left heart disease
3. Pulmonary hypertension owing to left heart disease and / or hypoxia
4. Chronic thromboembolic pulmonary hypertension (CTEPH)
5. Pulmonary hypertension with unclear multifactorial mechanisms

In patients with PAH an increase in pulmonary vascular resistance (PVR) and mean pulmonary arterial pressure (mPAP) can be found[1]. The clinical assessment of a patient suffering from PH can be performed with the WHO classification of the functional status[2].

Updated Clinical Classification of Pulmonary Hypertension (Nice, 2013)
1. Pulmonary arterial hypertension (PAH)
1.1. Idiopathic PAH
1.2. Heritable PAH
1.2.1. BMPR2
1.2.2. ALK-1, ENG, SMAD9, CAV1, KCNK3
1.2.3. Unknown
1.3. Drug and toxin induced
1.4. Associated with:
1.4.1. Connective tissue diseases
1.4.2. HIV infection
1.4.3. Portal hypertension
1.4.4. Congenital heart diseases
1.4.5. Schistosomiasis
1'. Pulmonary veno-occlusive disease (PVOD) and/or pulmonary capillary hemangiomatosis (PCH)
1". Persistent pulmonary hypertension of the newborn (PPHN)
2. Pulmonary hypertension due to left heart disease
2.1. Left ventricular systolic dysfunction
2.2. Left ventricular diastolic dysfunction
2.3. Valvular disease
2.4. Congenital/acquired left heart inflow/outflow tract obstruction and congenital cardiomyopathies
3. Pulmonary hypertension due to lung diseases and/or hypoxia
3.1. Chronic obstructive pulmonary disease
3.2. Interstitial lung disease
3.3. Other pulmonary diseases with mixed restrictive and obstructive pattern
3.4. Sleep-disordered breathing
3.5. Alveolar hypoventilation disorders
3.6. Chronic exposure to high altitude
3.7. Developmental lung diseases
4. Chronic thromboembolic pulmonary hypertension (CTEPH)
5. Pulmonary hypertension with unclear multifactorial mechanisms
5.1. Hematologic disorders: chronic hemolytic anemia, myeloproliferative disorders, splenectomy
5.2. Systemic disorders: sarcoidosis, pulmonary histiocytosis, lymphangioleiomyomatosis
5.3. Metabolic disorders: glycogen storage disease, Gaucher disease, thyroid disorders
5.4. Others: tumoral obstruction, fibrosing mediastinitis, chronic renal failure, segmental PH

Table 1.1 – Updated Clinical Classification of Pulmonary Hypertension (Nice 2013). BMPR = bone morphogenic protein receptor type II; CAV1 = caveolin-1; ENG = endoglin; HIV = human immunodeficiency virus; PAH = pulmonary arterial hypertension[54].

1.2.3 Pathology of pulmonary hypertension

1.2.3.1 Pulmonary arterial hypertension (PAH) and pulmonary veno-occlusive disease (PVOD)

According to the Nice 2013 classification shown above there are different pathological manifestations of the subtypes of PH. In PAH patients mainly the small pulmonary arteries are affected (< 500 µm of diameter). The cell wall shows intimal proliferation, medial hypertrophy and the adventitia becomes thicker. Inflammatory perivascular infiltrations can also be shown in this group. The lung veins are not affected. The pulmonary veno-occlusive disease (PVOD) group shows proliferation of the capillary bed, alveolar haemorrhage and inflammatory infiltrations in the pulmonary veins. The veins also gain a muscular wall. In this disease, pulmonary arteries can be affected, too[18].

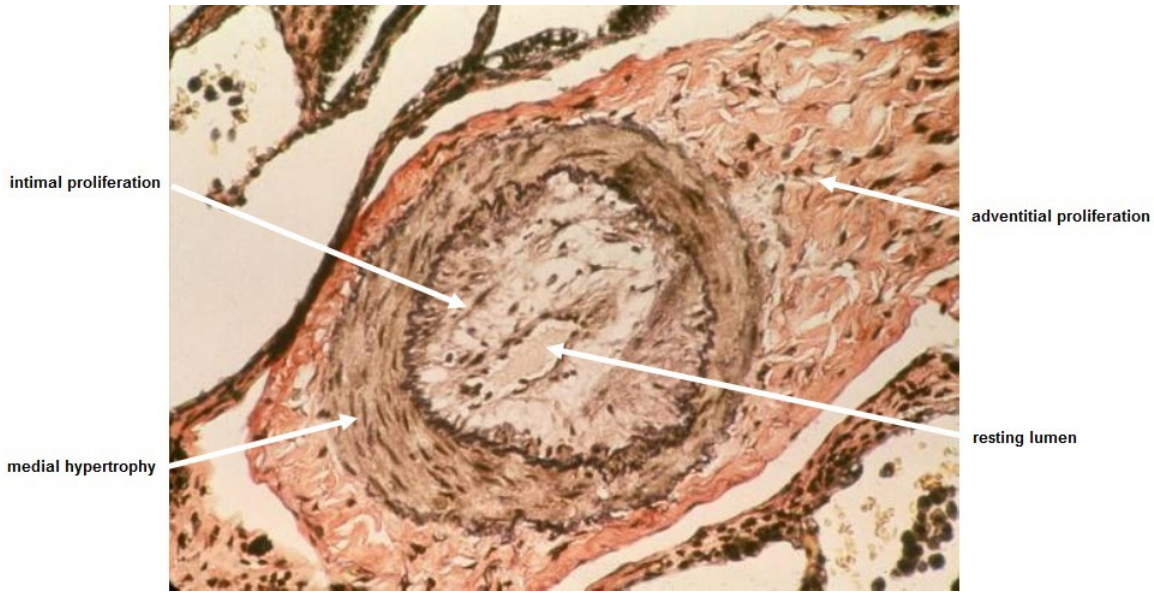

Figure 1.2 – Muscularized pulmonary artery from an IPAH patient[16].

1.2.3.2 Pulmonary hypertension owing to left heart disease

Pulmonary hypertension can also be caused by left heart disease and can increase vessel wall thickness, even in pulmonary veins. Other indicators are similar to PAH, for example alveolar haemorrhage and interstitial oedema. In PH due to left heart disease, pulmonary arteries can be affected, too[18].

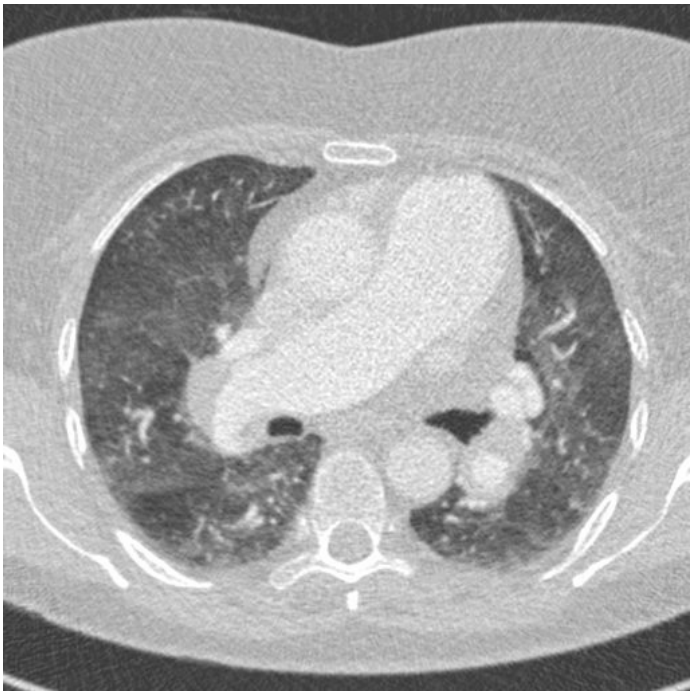

Figure 1.3 – Representative CT scan of a patient from our PH pilot study, suspect of PH caused by left heart disease.

1.2.3.3 Pulmonary hypertension owing to lung diseases and / or hypoxia

The most common diseases in this group are chronic obstructive pulmonary disease (COPD) and interstitial lung disease (ILD). Pathologic changes are similar to PAH. The distal pulmonary arteries become thicker because of medial hypertrophy and intimal proliferation. The proliferation leads to obstruction of the vessel. Furthermore, in these patients emphysema and fibrosis of the vascular bed can be observed[4][18].

Figure 1.4 – CT scan showing the lung of a patient from our PH pilot study with idiopathic pulmonary fibrosis (IPF).

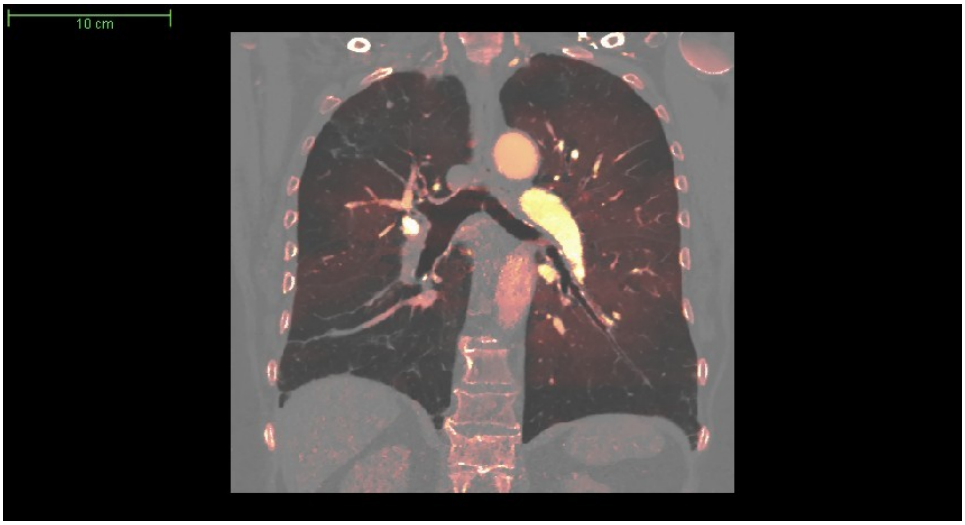

Figure 1.5 – DE-CT scan with overlay of denoised iodine perfusion CT scan of a patient from our PH pilot study with suspect CTEPH.

1.2.3.4 Chronic thromboembolic pulmonary hypertension (CTEPH)

CTEPH has a different morphology than the other subtypes and presents itself with organised thrombi that are connected to the media of the pulmonary arteries. These thrombi occlude the pulmonary perfusion, leading to the PH symptoms. The vasculature tries to compensate the loss of perfusion in affected areas with enlarged vessels leading to partial reperfusion and overperfusion of non-occluded areas[18].

1.2.3.5 Pulmonary hypertension with unclear multifactorial mechanisms

For this subgroup the pathomechanisms are yet to be clarified. Furthermore the morphology is presented in a very heterogeneous way[18].

1.2.4 Time to diagnosis and outcome

The outcome of the disease may vary depending on the subtype of PH and the severity of the symptoms present. PH is, regardless of progress in recent research, a fatal disease. Without proper treatment, the median survival rate for PAH patients for example is about 2.8 years. Approximately 68% survive the first year, 48% survive three years whereas only 34% are alive after 5 years after diagnosis[41]. A controlled trial of non-treatment is ethically impossible nowadays and the trial I referred to here was performed before the development of a therapy for PH. In a different cohort, patients received epoprostenol as treatment and the survival rates improved to 100% after the first year and 88% after the third year in WHO I or II. Whereas 77% were alive after the first year and 33% after the third year in WHO III, respectively[55]. Obviously a fast and accurate diagnosis of PH is needed to increase survival of patients suffering from PH. There is still a lack of biomarkers that have the power to show the pathologic mechanism, disease severity or treatment response in PH patients. Brain natriuretic peptide and N-terminal fragment of pro-brain natriuretic peptide are mentioned in current guidelines. Additionally, new potential biomarkers are currently investigated. Still there is the need for further research in the identification of promising disease markers[12].

1.2.5 Treatment of PH

The treatment of PH can vary greatly depending on the subgroup of PH diagnosed. Proper therapy slows down clinical worsening and can decrease the symptoms of the patients[21]. Furthermore, mortality can be decreased by 43% and hospitalizations reduced by 61% when comparing patients with therapy to patients with placebo. This has been shown on 23 different randomized controlled trials (RCTs) in PAH patients[19].

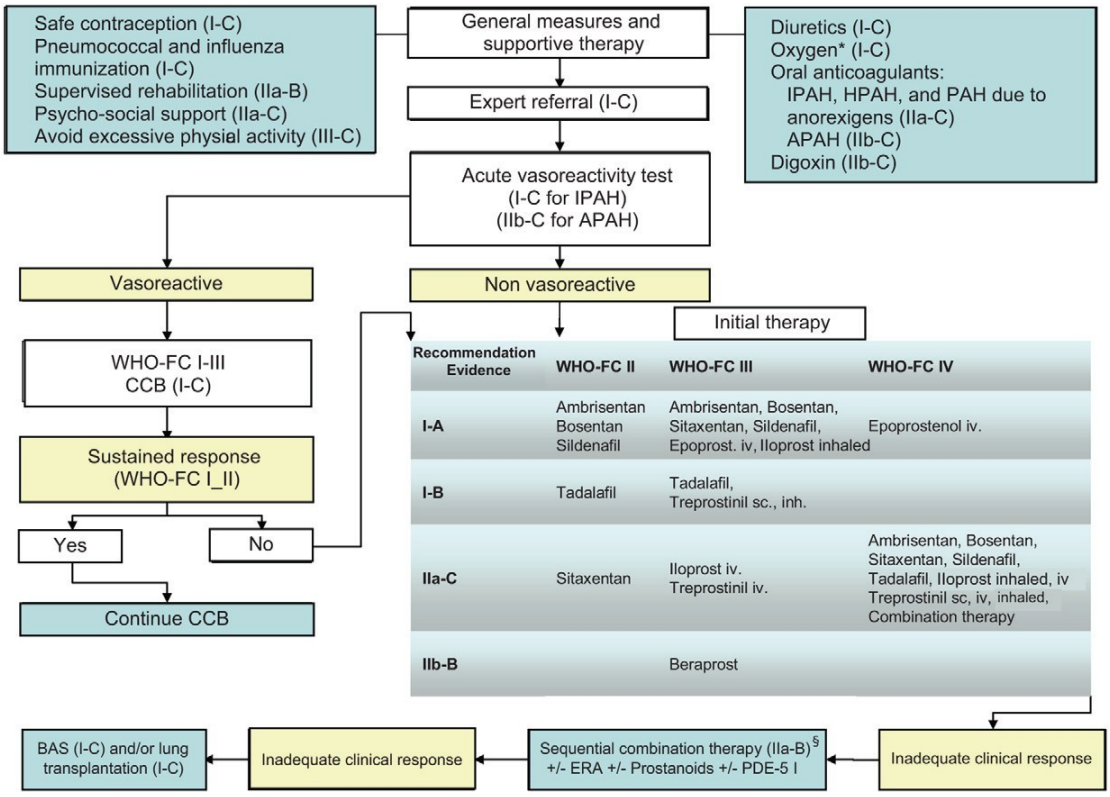

Figure 1.6 – Evidence-based treatment algorithm for patients with pulmonary arterial hypertension (for group 1 patients only)[21].

1.2.6 Non-invasive diagnosis of PH

PH is diagnosed by the invasive method of right heart catheterisation (RHC)[18, 54]. Although adverse events of RHC are rare in experienced centers, the development of non-invasive procedures could lead to a further reduction[29] or even replacement of RHC in follow-up examinations[58, 38, 45]. Recent literature shed some light on the possibilites of MRI examinations analysing blood velocity and blood flow patterns in the pulmonary trunk[51, 53]. Additionally, CT became a common procedure to rule out other lung diseases[8, 54]. Cardiac output (CO) is measured by RHC using a method called thermodilution[18, 20, 27]. CO is especially of clinical value because the therapy of the patient and listing for transplantation derives from it. Although there have been numerous evaluations of non-invasive CO determination by inert-gas rebreathing[28, 15, 42], impedance cardiography[62, 13, 47] and echocardiography[62, 44, 11, 14, 50], invasive thermodilution could not be replaced. Promising results have been reported recently by analysing the attenuation-time curves in the pulmonary artery and the ascending aorta from dynamic dual energy computed tomography scans (DECT)[48].

1.3 Computed tomography (CT)

Computed tomography (CT) nowadays has a wide range of diagnostic applications and has become a very valuable tool to differentiate disease types and subtypes. Thoracic CT provides high resolution and high contrast as a minimally invasive technique and is able to identify structural abnormilites in the lung[17]. For pulmonary hypertension patients CT of the chest resembles an important part of the evaluation of the disease[58]. Although the gold standard for diagnosis of PAH is right heart catheterization (RHC), chest CT scans can provide valuable information for ruling out other diseases in the first instance. However, the CT scans contain sufficient information to aid diagnosis of PH[49].

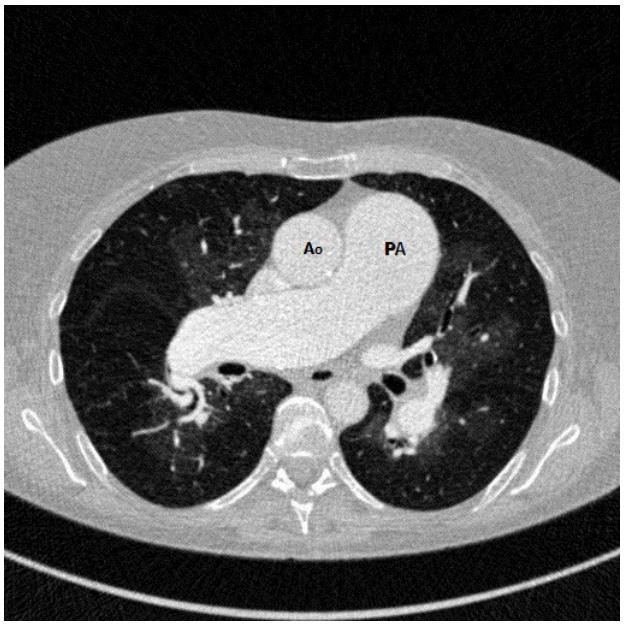

Figure 1.7 – A representative CT scan of a patient from our PH pilot study showing the aorta (Ao) and the dilated main pulmonary artery (PA).

1.3.1 CT for clinical PH diagnosis

When analysing a chest CT scan, there are two major points that give a hint for PAH. The first point is the dilation of the main pulmonary arteries. If they reach a diameter of 29 mm or greater the positive predictive value for PAH is 95% and the specifity is 89%[22]. The second point is the comparison between the diameter of the main pulmonary arteries and the aorta. It has been reported that, whenever the diameter of the main pulmonary arteries becomes greater than the diameter of the aorta, the positive predictive value for PAH is 95% and the specifity is 90%[22]. CT is a key procedure in diagnosis of pulmonary hypertension and is included twice in the diagnostic algorithm of pulmonary hypertension[18]. There is still work to be done to increase the diagnostic relevance of CT in pulmonary hypertension.

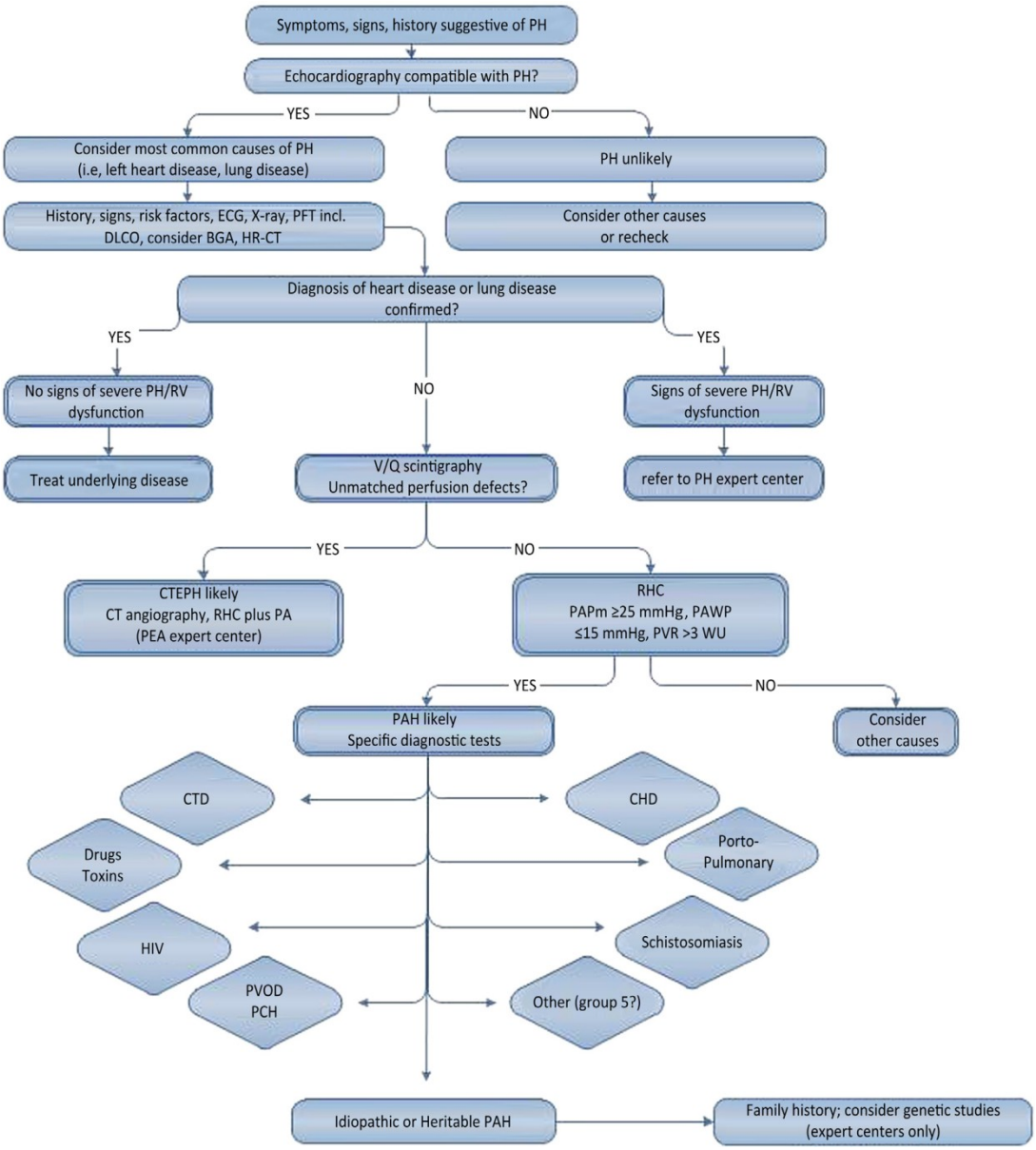

Figure 1.8 – Diagnostic Approach to Pulmonary Hypertension. BGA = blood gas analysis, CHD = congenital heart disease, CTD = connective tissue disease, CTEPH = chronic thromboembolic pulmonary hypertension, DLCO = diffusion capacity of the lung for carbon monoxide, ECG = electrocardiogram, HR-CT = high-resolution computed tomography, PA = pulmonary angiography, PAH = pulmonary arterial hypertension, PAPm = mean pulmonary arterial pressure, PAWP = pulmonary arterial wedge pressure, PCH = pulmonary capillary hemangiomatosis, PEA = pulmonary endarterectomy, PFT = pulmonary function testing, PH = pulmonary hypertension, PVOD = pulmonary veno-occlusive disease, PVR = pulmonary vascular resistance, RHC = right heart catheter, RV = right ventricle, V/Q = ventilation/perfusion, x-ray = chest radiograph[30].

1.3.2 Dual-energy computed tomography (DECT)

Dual-energy computed tomography (DECT) operates with two X-ray sources with different acceleration voltages and two detectors working simultaneously and allows the differentiation of tissue because the X-ray attenuation differs according to the tube voltage. This effect is very strong in contrast material such as xenon, barium or iodine. Therefore it is possible to measure iodine concentration on CT images[33]. This method has proven to be very sensitive in the diagnostic process of acute pulmonary embolism or CTEPH[10]. Recent studies also show the possibilites of lung perfused blood volume (PBV) in CTEPH patients by DECT and correlations with RHC parameters[43].

1.4 Objectives

The evaluation of the X-ray attenuation in the lung parenchyma by histogram analysis can give relevant values to quantify pathologic changes in the lung. The main goal is to identify diagnostically relevant parameters for PH and associated lung diseases, via correlation of the CT findings with patient clinical data. Furthermore, we aim to distinguish more common lung diseases like COPD or emphysema from PH in our histogram analysis, as they can show similar morphology in some regions of interest. We attempt to create an automated algorithm that evaluates the CT scan of the lung parenchyma and provides additional information for setting the diagnosis of PH. In the long run, our aim is to create a diagnostic tool with sensitivity and specifity comparable to the gold standard of RHC and therefore reduce the number of RHC a patient needs, especially in follow-up investigations.

Chapter 2

Materials and Methods

2.1 Patient population

The LBI pilot study was approved by the local ethics commitee. In the study 25 patients were enrolled and signed informed consent. All of the patients selected for the study already had a RHC for the diagnosis of PH at the Division of Pulmonology between May 2011 and January 2013. Most of the CT examinations were follow-up investigations to identify a change of pathological alterations. Furthermore, all of the CT examinations were done within 3 weeks of the RHC, with a median of 1 day (Table 3.2). There was no change in therapy during this time. Patients with renal failure, pregnancy, a recent diagnostic CT, known adverse reactions to iodinated contrast material and RHC with more than 1 month from the CT examination were excluded from the study.

2.2 Computed tomography (CT)

For the CT examinations a 128-slice dual-energy CT system (Somatom Definition Flash, Siemens, Forchheim, Germany) of the Diagnostikzentrum Graz was used. Patients were instructed to hold their breath in relaxed expiration or breathe slowly and shallowly during acquisition. The gantry rotation time was 0.5 s, the X-ray tubes were set to 100 kV / 53 mAs and 140 kV / 53 mAs with a 0.4 mm tin filter, respectively. 40 ml iodinated contrast material, Ultravist 370 mg/ml iodine (Bayer Schering Pharma Diagnostic Imaging, Leverkusen, Germany), have been injected at 5 ml/s flow rate. A medium-soft kernel (D30f) has been used for reconstruction of the images with 0.6 mm slice thickness. After the CT examination the anonymised data was transferred to an independent workstation.

2.3 Right heart catheterization (RHC)

All patients underwent RHC for follow-up or diagnostic reasons at the Division of Pulmonology, Medical University of Graz. A 7-F quadruple-lumen, balloon-tipped, flow-directed Swan-Ganz catheter (Baxter Healthcare Corp., Irvine, California) was used in a transjugular approach without transparency, performed by the same experienced medical personal.

2.4 Lung Perfused Blood Volume

To increase the discriminative power of our analysis we included perfused blood volume (PBV) data. It is important to mention that the DECT lung PBV data represents a snapshot of the lung perfusion at the given time point when the CT is taken[52]. Therefore it is not equivalent to the perfusion of the lung parenchyma, but it presents the iodine concentration distribution in the parenchyma.[63]

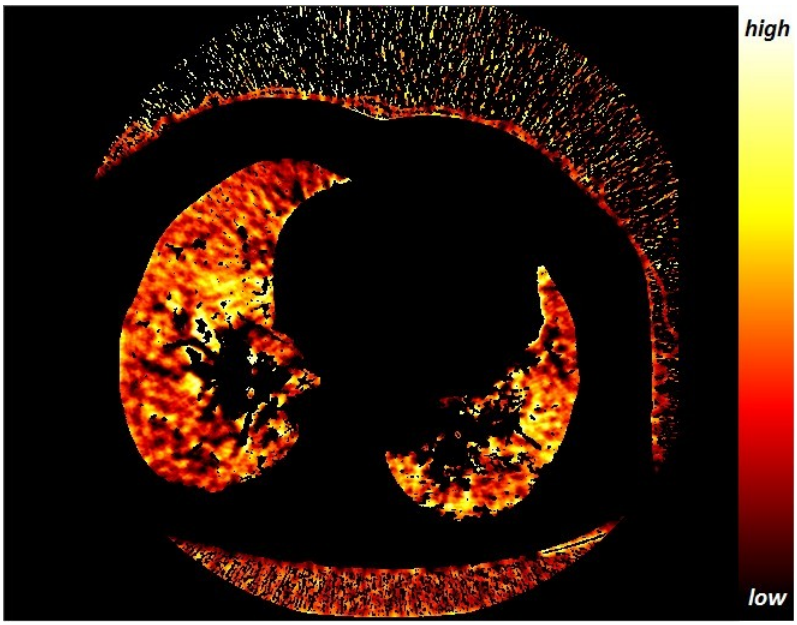

Figure 2.1 – A representative LungPBV scan of a patient from the PH pilot study with CTEPH after pulmonary endarterectomy.

2.5 Histogram analysis

The DECT images have been processed by an algorithm developed at the LBI LVR Graz. For the segmentation and histogram analysis we used MATLAB® R2010b (MathWorks Inc., Massachusetts, USA). In order to achieve an accurate segmentation of the lung parenchyma, the algorithm performed the following steps:

- 3D-segmentation of lung parenchyma
  - Denoising of the CT images and hounsfield units (HU) analysis
  - Isolation of the trachea and exclusion of vessels
  - Gradient calculation to sharpen the edges of lung parenchyma
  - Post-processing of the CT images to avoid segmentation failure and include fibrotic areas / emphysematous lung tissue
- Labeling of the segments found by the algorithm to differentiate left and right lung
- Quantitative analysis of lung parenchyma and lung vessels and visualization of the results

2.6 3D-segmentation of lung parenchyma

2.6.1 Denoising of the CT images and HU analysis

The first step in the development of the algorithm consisted in denoising the image. An automated in-house developed denoising algorithm was used to reduce the impact of noise on the analysis. Furthermore, filtering of the valuable lung parenchyma information had to be achieved. Therefore, a HU-threshold of -970 to -400 was set to exclude bones, fat and liquids, which all present HU at or above zero. As the image could also contain small objects outside of the thorax fulfilling these criteria, the perimeter of the thorax had to be identified to exclude for example the CT examination table from the segmentation. An important approach to achieve this goal was to identify the lung inside the thorax as two black objects, connected via the trachea, and remove all other objects (e.g. remaining noise, examination table) from the image.

2.6.2 Key steps in getting an accurate segmentation

The most important approach to get smooth borders of the lung parenchyma is the 3D ball analysis of the CT scan. All CT images are calculated simultaneously in a 3D array. The key steps of the segmentation consist of several image processing procedures. Dilation increases the border of all voxels in a binary image by a specific amount and geometric structure. In our algorithm we iteratively used balls of different sizes to clear the edges of lung parenchyma and allow the disconnection of the trachea without losing valuable information. The second procedure, called Erosion, works in the opposite direction, removing surrounding voxels of the binary image according to the 3D structure used (Figure 2.2). Again, balls of different sizes are used to delete artifacts in the CT scan. The third important procedure is the Connected Component analysis. With the help of Dilation and Erosion in combination, connected components in the whole CT scan can be identified. This iterative process reduces surroundings of the lung parenchyma, wrongly connected parts and even adds wrongly disconnected parts to the lung parenchyma. The algorithm stops when there are only 2 components left in the CT scan that are not connected to each other. This way identification of the two lungs of the patient is realized (see Figure 2.3).

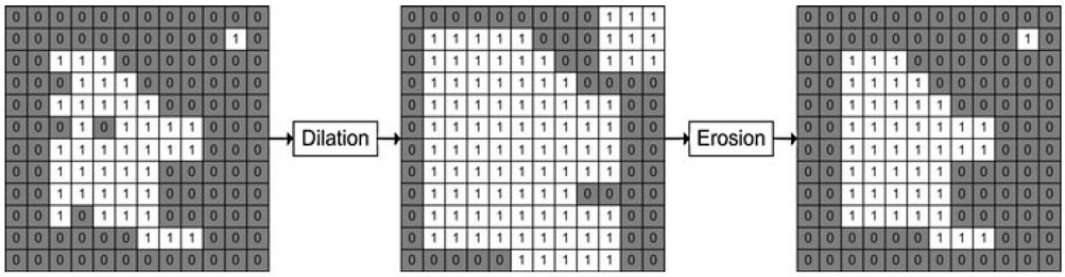

Figure 2.2 – Image processing procedures: Dilation and Erosion[64].

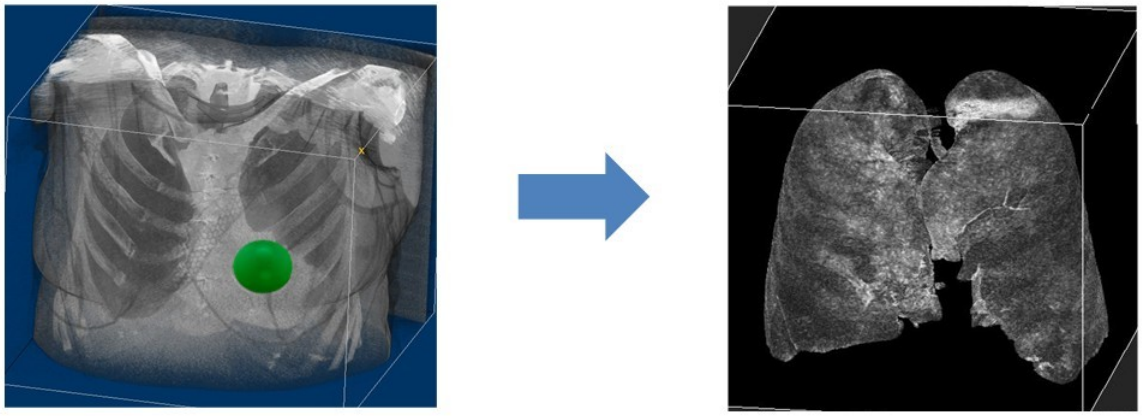

Figure 2.3 – Left: 3D array of all CT images of a representative CT scan, segmented by 3D balls of different sizes shown as green on the picture. Right: Lung parenchyma segmentation viewed in 3D.

2.6.3 Isolation of the trachea and exclusion of vessels

There have been different approaches to isolate the trachea from the CT scan. One of the steps for our algorithm was to identify the first big object reaching the thorax that is 3-dimensionally connected to the upper border of the image. The trachea was then marked and separated in small steps from the two lung lobes to avoid the loss of parenchyma information. As soon as the trachea lost connection to the two lung lobes, it was removed from the segmentation area. At this point we isolated both lungs with the lung vessels included.

2.6.4 Gradient calculation to sharpen the edges of lung parenchyma

To distinguish the small vessels from the lung parenchyma, it is not accurate enough to just erase the higher HU from the parenchyma, because there would be a loss of lung parenchyma and some vessels would still be present in the image. The later would be caused by darker pixels surrounding the vessel that dampen the brightness of the vessel in the scan. We calculated the gradient of the HU of the pixels in x-, y- and z-direction and removed points in the image whenever the change of the pixels in either x-, y- or z-direction was above a certain level, identifying a vessel path in the lung parenchyma.

2.6.5 Post-processing of the CT images

To avoid segmentation failure and include fibrotic areas / emphysematous lung tissue, more sophisticated approaches had to be developed. We used a region growing algorithm to check whether some parts of the lung were disconnected from the lung parenchyma (for example trapped air hidden behind fibrotic areas). Whenever such areas were found they were included in the lung parenchyma. By using this algorithm, we expected that the level of detail of our analysis will increase, especially in CTEPH patients. On the other hand we had to ensure that emphysematous tissue, represented as very dark areas below our -970 HU threshold, had not been removed. These areas should also yield valuable information, especially in atelectasia and COPD patients. An example of our post-processed segmentation images is shown in Figure 2.4.

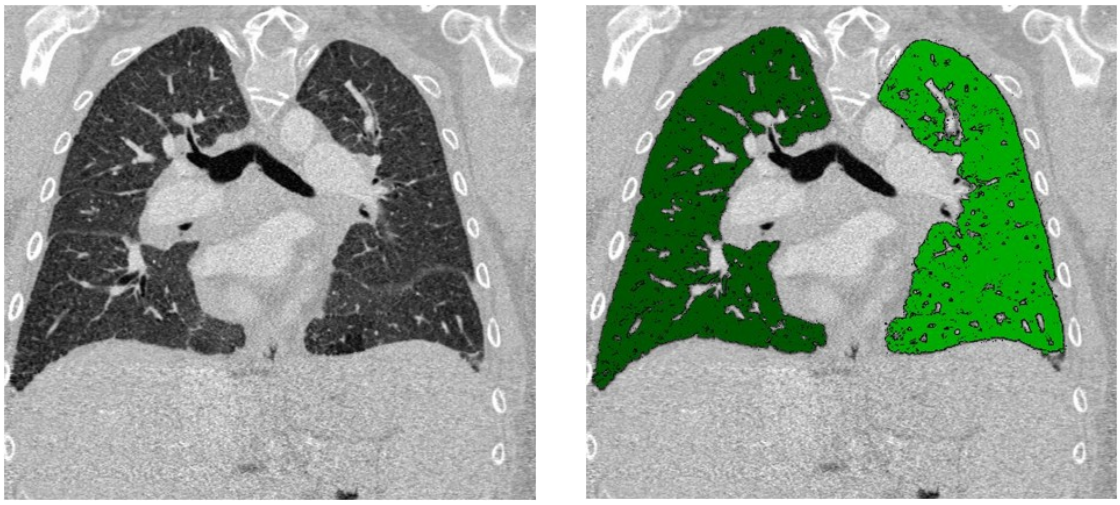

Figure 2.4 – CT scan image of a patient, (left) original image, (right) image after segmentation of lung parenchyma. Color coding: dark green = right lung, light green = left lung.

2.7 Quantitative analysis of the CT-scan data

2.7.1 Histogram

Histograms present the distribution of the values of a specific data set and can give a quick impression of how the data is scattered around distinct values. It can be used to visualize the relation between the values, for example the scattering of pixels with different hounsfield units (HU) in a CT image[57]. Two examples are shown on Figure 2.5 where the HU of two patients from the pilot study of the right and left lung can be seen.

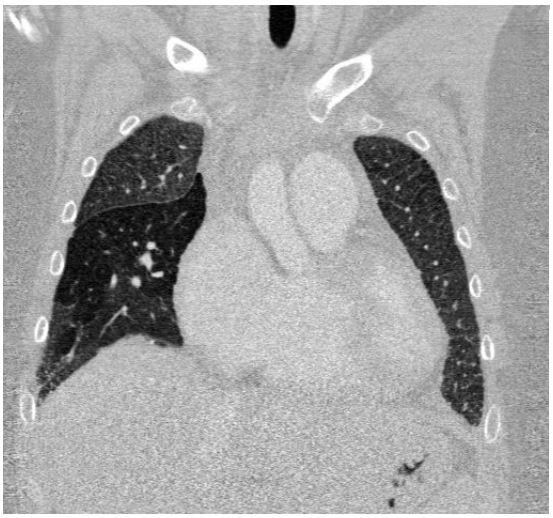

A

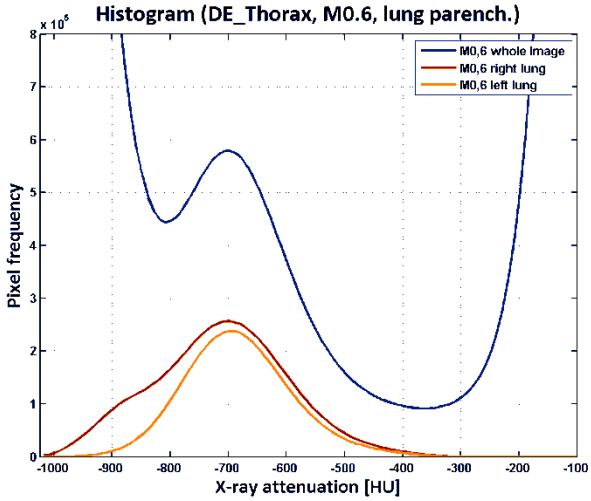

B

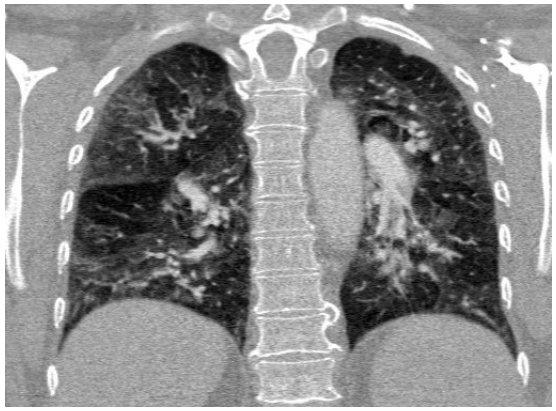

C

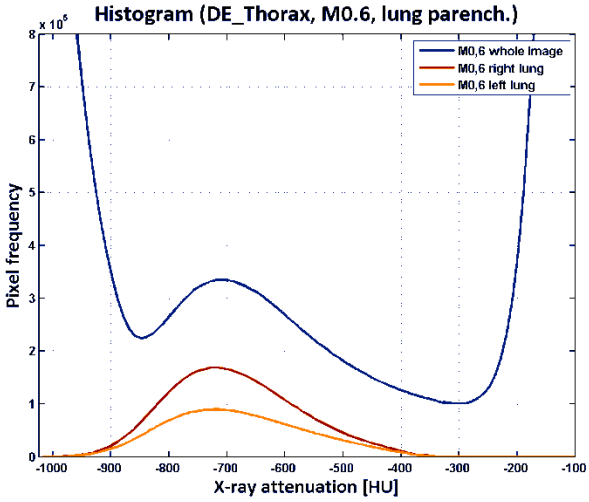

D

Figure 2.5 – A: Representative CT image of a patient from our PH pilot study. B: Histogram of the whole CT scan of the corresponding patient. C: Representative CT image of a patient of our PH pilot study. D: Histogram of the whole CT scan of the corresponding patient.

2.7.2 Mean lung attenuation (MLA)

The mean lung attenuation (MLA) $\overline{x}$ is calculated as the attenuation levels in Hounsfield Units (HU) of the lung tissue in the whole scan[4]. It has been shown that this basic histogram parameter correlates with the values of pulmonary function tests (PFTs) in interstitial lung disease (ILD) patients[25].

$$\overline{x} = \frac{1}{n}\sum_{i=1}^{n} k$$

n … sample size

k … value of items

2.7.3 Skewness

The skewness ν can describe the asymmetry of a histogram. Skewness is computed with the following formula:

$$\nu = \frac{1}{n}\sum_{i=1}^{n}\left(\frac{x_i - \overline{x}}{s}\right)^3$$

n … sample size

s … standard deviation

If the skewness is 0, the histogram is perfectly symmetric. A histogram that is skewed to the left has negative skewness values, whereas when skewed to the right the values are positive[37].

2.7.4 Kurtosis

Kurtosis ω is a parameter that provides information about the sharpness of the peak of a histogram. Kurtosis is computed with the following formula:

$$\omega = \frac{1}{n}\sum_{i=1}^{n}\left(\frac{x_i - \overline{x}}{s}\right)^4 - 3$$

n … sample size

s … standard deviation

Histograms having the shape of a normal distribution show the kurtosis of 0. A sharper curve has a kurtosis greater than 0, whereas a kurtosis below 0 represents a flatter curve[37].

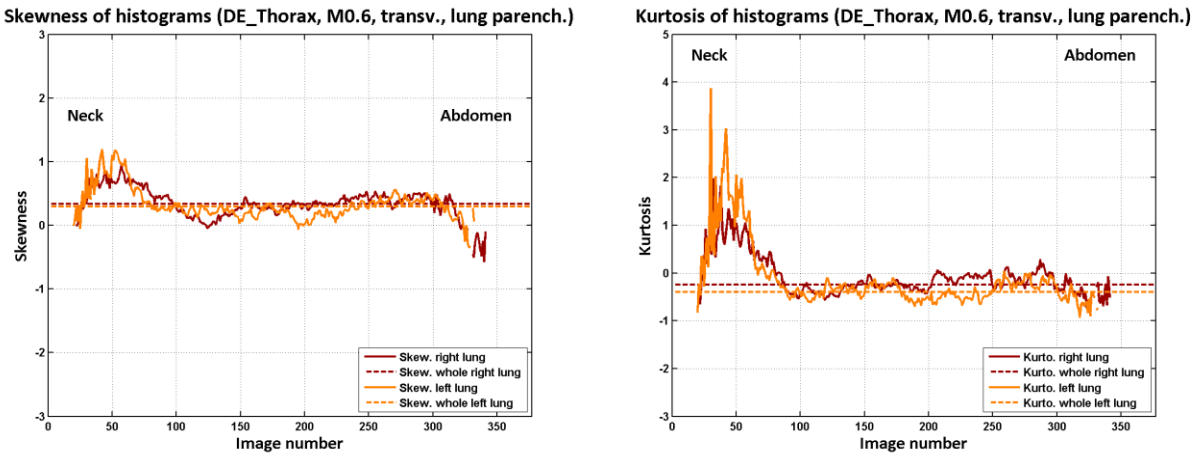

Figure 2.6 – Left: Skewness of a representative Hounsfield unit based CT histogram by image number. Right: Kurtosis of a histogram by image number.

2.7.5 Full-width at half-maximum (FWHM)

The full-width at half maximum (FWHM) can give valuable information about the scattering of the values either side from the peak. Full-width at half-maximum is calculated as follows:

$$FWHM = \frac{1}{s\sqrt{2\pi}} \exp\,[-\frac{(x -}{}$$

s…standard deviation

2.7.6 Normalized peak height (N_peak)

Because of the different lung sizes of the different patients, the height of the peak was not a valid parameter to analyse. Therefore we normalized the peak height by the sum of all voxels of the specific lung.

$$N\_peak = \frac{peak\_height}{\sum voxels}$$

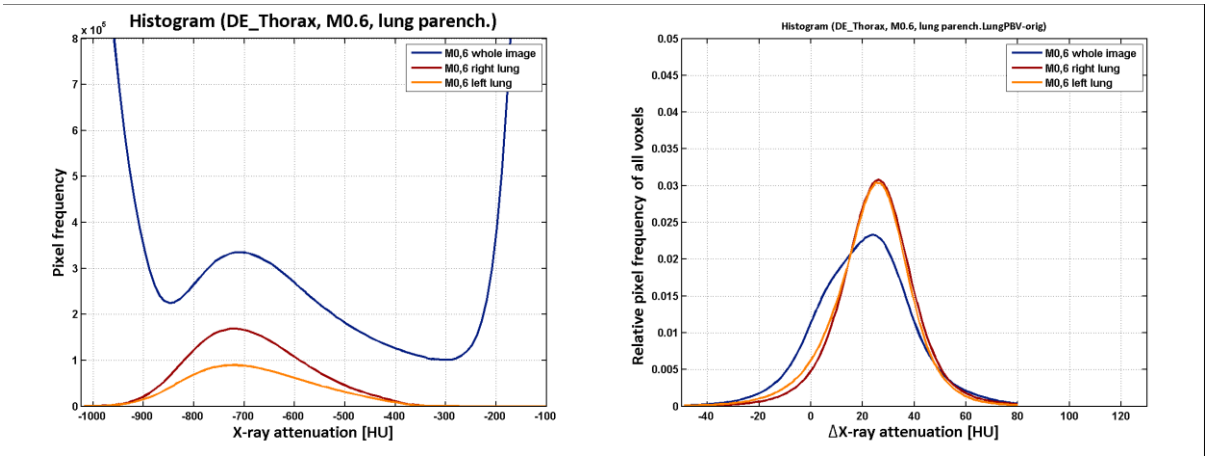

Figure 2.7 – Left: Full-width at half-maximum of a histogram. The FWHM is delineated by the left and right dark and light green dashed lines, respectively. Right: Normalized peak height of a histogram.

2.7.7 Statistical analysis

Statistical analysis was performed in GraphPad Prism (Version 5.04, GraphPad Software, Inc., La Jolla, CA, USA). Correlations between DECT and RHC-derived parameters were calculated using Spearman correlation; differences between PH and non-PH patients were determined using a t-test. We considered P values ≤ 0.05 significant.

Chapter 3

Results

3.1 Patient characteristics

Twenty-five (n=25) patients (female:male = 15:10) were enrolled in a clinical PH pilot study. Four patients had to be excluded from the analysis, three patients (Patient 10, Patient 21, Patient 22) because the data acquisition failed or has not been achieved in 1 month after RHC. One patient had to be excluded because the segmentation algorithm failed to distinguish the two lungs (Patient 19). Therefore the statistical analysis was performed on twenty-one patients.

Patient characteristics	All Patients	No PH	PH
Number of patients	21	5	16
Age [years]	60 ± 14 (27 - 76)	56 ± 7 (50 - 68)	61 ± 16 (27 - 76)
BSA [m^2]	1.9 ± 0.3 (1.5 - 2.7)	1.8 ± 0.1 (1.6 - 1.9)	1.9 ± 0.3 (1.5 - 2.7)
mPAP [mmHg]	37 ± 16 (14 - 66)	16 ± 2 (14 - 19)	44 ± 12 (26 - 66)
PAWP [mmHg]	9 ± 3 (3 - 15)	8 ± 3 (5 - 11)	9 ± 3 (3 - 15)
CO [l/min]	4.5 ± 1.1 (2.9 - 7.8)	5.3 ± 1.5 (4.3 - 7.8)	4.2 ± 0.9 (2.9 - 5.7)
PVR [dyn s cm^{-5}]	556 ± 385 (75 - 1416)	112 ± 24 (75 - 131)	695 ± 334 (226 - 1416)
$AVDO_2$ [vol%]	4.9 ± 1.0 (2.4 - 6.4)	4.1 ± 0.5 (3.3 - 4.7)	5.2 ± 1.0 (2.4 - 6.4)
art SO_2 [%]	94 ± 3 (89 - 98)	96 ± 1 (95 - 98)	93 ± 2 (89 - 98)
ven SO_2 [%]	67 ± 8 (50 - 84)	73 ± 2 (71 - 76)	65 ± 8 (50 - 84)

Table 3.1 – Patient characteristics (BSA = body surface area, mPAP = mean pulmonary arterial pressure, PAWP = pulmonary artery wedge pressure, CO = cardiac output, PVR = pulmonary vascular resistance, $AVDO_2$ = arteriovenous oxygen difference, $artSO_2$ = arterial oxygen saturation, $venSO_2$ = venous oxygen saturation).

3.1.1 Associated diseases

We analysed our patient population based on RHC parameters and clinical diagnosis. Therefore we wanted to investigate underlying diseases.

Patient ID	Indication for RHC	Date of RHC	Indication for CT	Date of CT	Diagnosis
LBI_Pilot01	progressing symptoms	20/06/2011	control of lung fibrosis	21/06/2011	PH - Lung
LBI_Pilot02	planned start of PAH therapy	04/07/2011	exclusion of lung parenchymal disease	05/07/2011	IPAH
LBI_Pilot03	pulmonary endarterectomy	02/10/2011	exclusion of lung parenchymal disease	03/10/2011	CTEPH (after PEA - rest PH)
LBI_Pilot04	pulmonary endarterectomy	07/10/2011	exclusion of lung parenchymal disease	25/10/2011	CTEPH (after PEA - rest PH)
LBI_Pilot05	suspected PH	13/10/2011	suspected progression of scleroderma lung disease	14/10/2011	Scleroderma (no PH)
LBI_Pilot06	suspected PH	03/11/2011	suspected progression of scleroderma lung disease	04/11/2011	Scleroderma (no PH)
LBI_Pilot07	suspected PH	08/11/2011	control of lung fibrosis	09/11/2011	ILD (no PH)
LBI_Pilot08	suspected PH	13/11/2011	suspected progression of scleroderma lung disease	14/11/2011	Scleroderma (no PH)
LBI_Pilot09	progressing symptoms	21/11/2011	exclusion of lung parenchymal disease	22/11/2011	CTEPH
LBI_Pilot10	pulmonary endarterectomy	19/01/2012	exclusion of lung parenchymal disease	20/01/2012	ex CTEPH (after PEA - no PH)
LBI_Pilot11	progressing symptoms	30/01/2012	exclusion of lung parenchymal disease	31/01/2012	PH bei OSAS
LBI_Pilot12	suspected PH	15/02/2012	exclusion of lung parenchymal disease	16/02/2012	CTEPH
LBI_Pilot13	suspected PH	08/03/2012	exclusion of lung parenchymal disease	09/03/2012	PH - lung dis.
LBI_Pilot14	suspected PH	15/03/2012	exclusion of lung parenchymal disease	16/03/2012	PAH
LBI_Pilot15	pulmonary endarterectomy	07/05/2012	exclusion of lung parenchymal disease	08/05/2012	CTEPH (after PEA - rest PH)
LBI_Pilot16	suspected PH	10/05/2012	exclusion of lung parenchymal disease	11/05/2012	PAH - cong. heart dis.
LBI_Pilot17	suspected PH	14/05/2012	exclusion of lung parenchymal disease	15/05/2012	CTEPH
LBI_Pilot18	pulmonary endarterectomy	12/06/2012	exclusion of lung parenchymal disease	13/06/2012	CTEPH (after PEA - rest PH)
LBI_Pilot19	progressing symptoms	12/07/2012	control of severe lung emphysema	13/07/2012	PH - lung dis.
LBI_Pilot20	progressing symptoms	30/07/2012	control of lung fibrosis	01/08/2012	PAH
LBI_Pilot21	suspected PH	02/02/2012	exclusion of lung parenchymal disease	20/09/2012	St.p. PAE (no PH)
LBI_Pilot22	suspected PH	24/09/2012	exclusion of lung parenchymal disease	01/10/2012	PAH-PoPH
LBI_Pilot23	progressing symptoms	26/09/2012	exclusion of lung parenchymal disease	09/10/2012	PH-Schlafapnoe
LBI_Pilot24	suspected PH	04/12/2012	exclusion of lung parenchymal disease	06/12/2012	IPAH
LBI_Pilot25	suspected PH	07/01/2013	exclusion of lung parenchymal disease	08/01/2013	Scleroderma (no PH)

Table 3.2 – Associated diseases of all patients in the clinical PH pilot study (PH = pulmonary hypertension, IPAH = idiopathic pulmonary arterial hypertension, PEA = pulmonary endarterectomy, ILD = interstitial lung disease, OSAS = obstructive sleep apnoea syndrome).

3.1.2 Bolus timing

The CT image acquisition was based on the estimated time for the contrast material bolus injection needed to represent the lung parenchyma best. Bolus timing for the thoracic contrast enhanced CT examination was determined from a dynamic CT sequence carried out prior to the thoracic CT examination. To check whether the bolus timing in our patients was correct, we quantified the average X-ray attenuation in the pulmonary artery and the left atrium and calculated the ratio of AttPA over AttLA (see Table 3.3). Values range between 0.5 and 1.82 resulting in proper performed timing for optimal pulmonary enhancement.

Patient	Att PA [HU]	Att LA [HU]	Ratio
LBI_Pilot01	179	204	0.877
LBI_Pilot02	332	302	1.099
LBI_Pilot03	368	216	1.704
LBI_Pilot04	175	237	0.738
LBI_Pilot05	173	343	0.504
LBI_Pilot06	160	320	0.500
LBI_Pilot07	341	319	1.069
LBI_Pilot08	217	354	0.613
LBI_Pilot09	351	314	1.118
LBI_Pilot10	129	265	0.487
LBI_Pilot11	156	174	0.897
LBI_Pilot12	241	236	1.021
LBI_Pilot13	168	269	0.625
LBI_Pilot14	261	313	0.834
LBI_Pilot15	244	309	0.790
LBI_Pilot16	279	247	1.130
LBI_Pilot17	109	267	0.408
LBI_Pilot18	372	350	1.063
LBI_Pilot19	217	276	0.786
LBI_Pilot20	186	302	0.616
LBI_Pilot21	245	251	0.976
LBI_Pilot23	295	162	1.821
LBI_Pilot24	297	300	0.990
LBI_Pilot25	264	293	0.901

Table 3.3 – Bolus timing (PA = pulmonary artery, LA = left atrium).

3.2 Lung Segmentation

We developed an automatic algorithm to isolate lung parenchyma and lung vessels. This has been achieved in 3D by using thresholds. For lung parenchyma, the HU of -970 to -400 were found sufficient. After the deletion of artifacts from outside of the thorax, the trachea had to be removed from the segmentation. To remove the trachea we used different binary image masks and image processing procedures like erosions and dilations. Furthermore we computed the gradient in x, y and z directions to get clean borders between vessels and parenchyma.

One example of the algorithm is shown on Figure 3.1, where the two separated and identified lungs are depicted (orange = right lung, yellow = left lung).

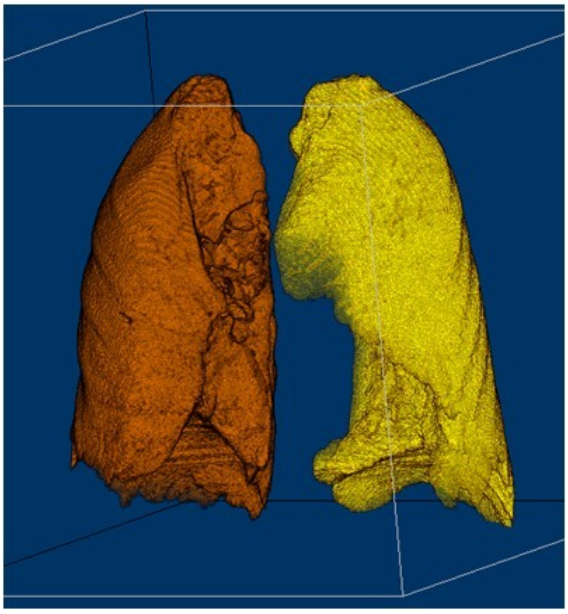

Figure 3.1 – 3D segmentation of the right lung (orange) and the left lung (yellow) from a representative patient from our PH pilot study.

3.2.1 Advantages

The algorithm we created works fully automatic. There is no user interaction necessary for segmenting lung parenchyma and vessels. Additionally we decided to increase the level of detail of the segmentation by using 3D dependent methods. There are numerous image processing functions in 2D and 3D and it is obvious that by taking the whole CT scan into account to differentiate between parenchyma and surrounding tissue, one can expect more detailed results.

3.2.2 Disadvantages

Although the 3D segmentation process of the lung parenchyma provides a lot of details, the computational effort for this task remains high. At the current status we achieved an average of 20 minutes of processing time for one patient at a standard workstation.

3.2.3 Quality control of segmentation

We performed visual inspection on all CT images having the segmentation as semi-transparent overlay. All patients had satisfying segmentations except Pilot19, which was therefore excluded from the analysis.

3.3 HU histogram analysis

Detailed analysis of all previously mentioned histogram parameters (Section 2.7) has been performed on our datasets. In table 3.4 we represent all individual values for our 6 readouts of the histograms, separated for the left and right lung, respectively.

	Mean		STD		Skew		Kurt		FWHH		N_Peak	
	Left	Right	Left	Right	Left	Right	Left	Right	Left	Right	Left	Right
Pilot01	-684.755	-712.461	90.665	111.161	0.125	-0.025	-0.166	-0.511	220.589	281.039	4.422	3.542
Pilot02	-817.134	-821.584	95.809	89.921	1.015	1.093	0.836	1.216	183.723	170.542	5.140	5.737
PIlot03	-715.408	-757.672	102.390	102.435	0.177	0.569	-0.466	-0.162	265.711	228.022	3.747	4.227
Pilot04	-714.877	-744.082	102.925	101.527	0.373	0.512	-0.593	-0.241	265.670	233.824	3.949	4.089
Pilot05	-741.869	-752.022	90.665	88.004	0.810	0.954	0.294	1.392	172.760	167.788	5.462	5.703
Pilot06	-797.302	-819.452	94.423	85.677	1.047	1.158	1.588	1.745	180.067	167.549	5.281	5.768
Pilot07	-861.464	-873.355	76.008	74.132	1.742	1.870	4.352	5.005	136.209	132.392	7.285	7.504
Pilot08	-826.098	-830.767	80.911	77.134	1.510	1.575	2.957	3.468	138.388	134.523	7.100	7.425
Pilot09	-748.700	-741.581	103.005	108.204	0.488	0.367	-0.230	-0.427	240.827	259.847	4.010	3.778
Pilot10	-842.329	-842.862	71.972	71.591	1.574	1.498	4.031	3.741	136.437	139.244	7.418	7.258
Pilot11	-706.434	-730.426	112.512	110.950	0.163	0.304	-0.218	-0.513	322.204	286.019	3.219	3.491
Pilot12	-841.631	-875.699	79.787	73.182	1.455	2.005	3.025	5.574	150.389	122.769	6.456	8.409
Pilot13	-847.135	-840.182	86.349	93.349	1.424	1.327	2.512	1.853	155.689	161.655	6.121	5.751
Pilot14	-711.523	-726.210	107.162	101.419	0.173	0.369	-0.597	-0.347	294.960	243.252	3.497	3.995
Pilot15	-842.573	-847.941	77.981	78.128	1.541	1.535	3.450	3.461	143.584	147.664	6.862	6.629
Pilot16	-794.412	-802.997	90.397	79.806	1.014	1.214	1.098	2.159	169.457	147.200	5.558	6.608
Pilot17	-814.729	-824.724	89.041	80.991	1.135	1.293	1.526	2.409	169.515	153.145	5.616	6.355
Pilot18	-874.762	-868.530	71.767	73.831	2.062	1.945	6.061	5.301	123.191	125.846	8.344	8.153
Pilot20	-846.370	-846.526	94.426	92.703	1.274	1.281	1.694	1.812	175.608	176.276	5.337	5.323
Pilot21	-788.484	-748.434	108.796	109.693	0.816	0.436	-0.049	-0.555	184.562	291.181	5.012	3.650
Pilot23	-788.818	-786.887	92.857	91.278	0.801	0.785	0.704	0.735	194.223	190.955	4.891	4.980
Pilot24	-685.830	-687.956	106.803	103.291	-0.019	0.038	-0.669	-0.599	315.295	295.768	3.281	3.485
Pilot25	-755.390	-774.832	94.159	92.113	0.606	0.749	0.219	0.549	199.027	192.485	4.741	4.921

Table 3.4 – HU histogram data of all histogram parameters previously described. STD = standard deviation, Skew = skewness, Kurt = kurtosis, FWHM = full-width at half-maximum, N_peak = normalized peak.

3.3.1 Correlations with HU histogram data

Color code:	Spearman r	≥ 0.50	≥ 0.60	≥ 0.70	≥ 0.75	≥ 0.80
	P value (two-tailed)	≤ 0.05	≤ 0.01	≤ 0.001	≤ 0.0001	

		leftMLA	left skewness	left kurtosis	left FWHM	left N_peak
meanPAP	Spearman r	0.1478	-0.2662	-0.2475	0.3178	-0.3149
	95% confidence interval	-0,3042 to 0,5455	-0,6266 to 0,1880	-0,6143 to 0,2072	-0,1331 to 0,6597	-0,6579 to 0,1362
	P value (two-tailed)	0.5115	0.2311	0.2667	0.1496	0.1534
Body surface area - Dubois	Spearman r	0.1282	-0.05138	0.06042	0.03444	-0.002823
	95% confidence interval	-0,3223 to 0,5313	-0,4734 to 0,3899	-0,3821 to 0,4804	-0,4041 to 0,4602	-0,4349 to 0,4303
	P value (two-tailed)	0.5697	0.8204	0.7894	0.8791	0.9901
Age	Spearman r	-0.2445	0.2061	0.1169	-0.1711	0.1722
	95% confidence interval	-0,6123 to 0,2103	-0,2486 to 0,5864	-0,3325 to 0,5230	-0,5621 to 0,2824	-0,2813 to 0,5629
	P value (two-tailed)	0.2728	0.3575	0.6045	0.4465	0.4434
SVR	Spearman r	-0.1993	0.1112	0.07058	-0.1124	0.1056
	95% confidence interval	-0,5817 to 0,2553	-0,3376 to 0,5188	-0,3734 to 0,4882	-0,5197 to 0,3366	-0,3426 to 0,5147
	P value (two-tailed)	0.3738	0.6221	0.7549	0.6186	0.64
PVR	Spearman r	0.1711	-0.3032	-0.3021	0.3506	-0.3529
	95% confidence interval	-0,2824 to 0,5621	-0,6505 to 0,1489	-0,6498 to 0,1501	-0,09657 to 0,6801	-0,6814 to 0,09401
	P value (two-tailed)	0.4465	0.1701	0.1718	0.1096	0.1072
AVDO2	Spearman r	0.3326	-0.4342	-0.3755	0.476	-0.4591
	95% confidence interval	-0,1168 to 0,6689	-0,7297 to -0,002029	-0,6952 to 0,06814	0,05469 to 0,7534	-0,7439 to -0,03306
	P value (two-tailed)	0.1305	0.0435	0.0851	0.0251	0.0316
art SO2	Spearman r	-0.3615	0.4682	0.4535	-0.597	0.5835
	95% confidence interval	-0,6867 to 0,08427	0,04472 to 0,7491	0,02609 to 0,7408	-0,8183 to -0,2217	0,2018 to 0,8113
	P value (two-tailed)	0.0983	0.028	0.034	0.0034	0.0044
ven SO2	Spearman r	-0.4704	0.5731	0.5822	-0.6375	0.6228
	95% confidence interval	-0,7503 to -0,04744	0,1869 to 0,8059	0,1999 to 0,8106	-0,8388 to -0,2829	0,2604 to 0,8314
	P value (two-tailed)	0.0272	0.0053	0.0045	0.0014	0.002

Table 3.5 – HU histogram Spearman correlations with RHC parameters, left lung.

Color code:	Spearman r	≥ 0.50	≥ 0.60	≥ 0.70	≥ 0.75	≥ 0.80
	P value (two-tailed)	≤ 0.05	≤ 0.01	≤ 0.001	≤ 0.0001	

		rightMLA	right skewness	right kurtosis	right FWHM	right N_peak
meanPAP	Spearman r	0.1206	-0.2424	-0.2804	0.3348	-0.3144
	95% confidence interval	-0,3291 to 0,5258	-0,6109 to 0,2124	-0,6358 to 0,1732	-0,1144 to 0,6703	-0,6575 to 0,1368
	P value (two-tailed)	0.5928	0.277	0.2063	0.1278	0.1542
Body surface area - Dubois	Spearman r	0.0288	-0.06494	-0.0367	0.07171	-0.07058
	95% confidence interval	-0,4089 to 0,4557	-0,4839 to 0,3783	-0,4619 to 0,4023	-0,3724 to 0,4891	-0,4882 to 0,3734
	P value (two-tailed)	0.8988	0.774	0.8712	0.7511	0.7549
Age	Spearman r	-0.1779	0.1779	0.17	-0.1903	0.1948
	95% confidence interval	-0,5668 to 0,2759	-0,2759 to 0,5668	-0,2834 to 0,5613	-0,5755 to 0,2640	-0,2596 to 0,5786
	P value (two-tailed)	0.4284	0.4284	0.4495	0.3963	0.385
SVR	Spearman r	-0.2084	0.1767	0.1643	-0.127	0.1169
	95% confidence interval	-0,5879 to 0,2464	-0,2770 to 0,5660	-0,2888 to 0,5573	-0,5305 to 0,3233	-0,3325 to 0,5230
	P value (two-tailed)	0.3521	0.4314	0.465	0.5732	0.6045
PVR	Spearman r	0.1677	-0.2818	-0.3145	0.3586	-0.3461
	95% confidence interval	-0,2856 to 0,5597	-0,6367 to 0,1717	-0,6576 to 0,1366	-0,08760 to 0,6849	-0,6773 to 0,1017
	P value (two-tailed)	0.4557	0.204	0.154	0.1013	0.1146
AVDO2	Spearman r	0.2976	-0.4241	-0.4421	0.5031	-0.4952
	95% confidence interval	-0,1549 to 0,6469	-0,7238 to 0,01043	-0,7343 to -0,01181	0,09016 to 0,7684	-0,7641 to -0,07970
	P value (two-tailed)	0.1786	0.0492	0.0394	0.017	0.0191
art SO2	Spearman r	-0.3186	0.462	0.5275	-0.5885	0.5524
	95% confidence interval	-0,6602 to 0,1322	0,03680 to 0,7456	0,1230 to 0,7817	-0,8139 to -0,2092	0,1574 to 0,7950
	P value (two-tailed)	0.1485	0.0304	0.0116	0.004	0.0077
ven SO2	Spearman r	-0.4726	0.5731	0.6081	-0.6522	0.6443
	95% confidence interval	-0,7515 to -0,05033	0,1869 to 0,8059	0,2382 to 0,8240	-0,8461 to -0,3059	0,2935 to 0,8421
	P value (two-tailed)	0.0263	0.0053	0.0027	0.001	0.0012

Table 3.6 – HU histogram Spearman correlations with RHC parameters, right lung.

In the HU histogram analysis significant correlations between all oxygen exchange parameters and FWHM or normalized peak has been found. The individual relations of artSO_2 are depicted on Figure 3.2. Arterial oxygen saturation (art SO_2) had negative correlations with FWHM of ρ=-0.60 (p=0.0034) and ρ=-0.59 (p=0.004) of the left and right lung, respectively. Normalized peak values in the left lung had ρ=0.5835 (p=0.0044) and ρ=0.5524 (p=0.0077) in the right lung. Venous oxygen saturation (ven SO2) were correlated with FWHM having ρ=-0.6375 (p=0.0014) and ρ=-0.6522 (p=0.001) of the left and right lung, respectively. Normalized peak values in the left lung were correlated with ρ=0.6228 (p=0.002) in the left lung and ρ=0.6443 (p=0.0012) in the right lung. No correlations could be observed with body surface area (BSA), age and systemic vascular resistance (SVR). There was also no significant correlation with mPAP or WHO class.

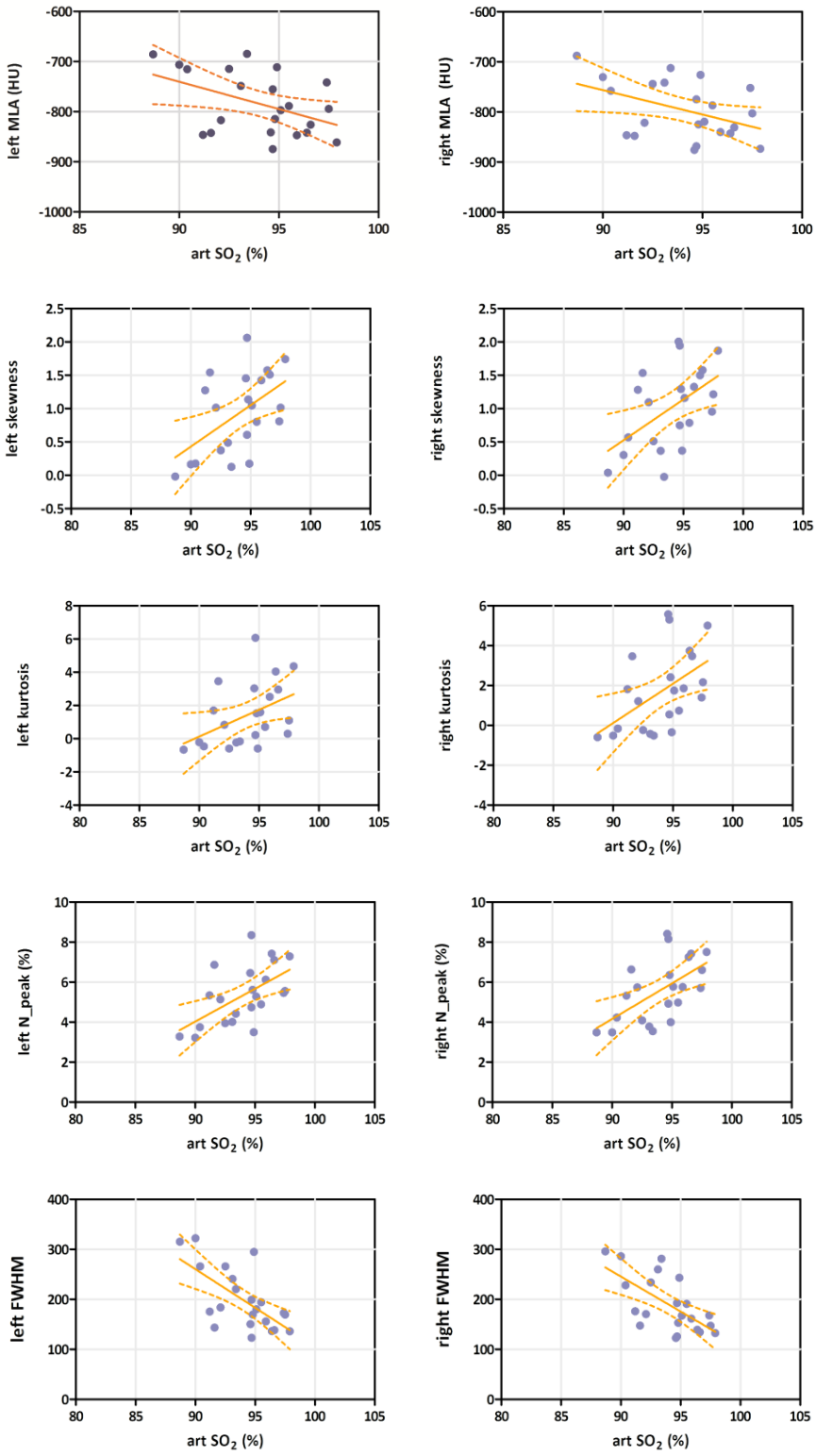

Figure 3.2 – Correlations of HU histogram data with art SO_2.

Lung function parameters also showed linear correlation with quantitative parameters. Total lung capacity (TLC) had linear relation with mean lung attenuation (MLA) of R^2=0.3886 (p=0.01) and R^2=0.32 (p=0.022) for left and right lung, respectively. The individual relations are depicted on Figure 3.3.

Color code:	Lin.reg. R2	≥ 0.25	≥ 0.35	≥ 0.50	≥ 0.60	≥ 0.70
	P value (two-tailed)	≤ 0.05	≤ 0.01	≤ 0.001	≤ 0.0001	

		left MLA	left skewness	left kurtosis	left FWHM	left N_peak
FEV1/FVC	R square	0.3524	0.2552	0.1359	0.1808	0.1219
	P value	0.012	0.0386	0.1454	0.0888	0.1695
DLCOcVA	R square	0.001644	0.0002031	0.0004959	0.007718	0.001156
	P value	0.8859	0.9598	0.9372	0.7555	0.9043
FEV1	R square	0.03066	0.06445	0.1266	0.004494	0.09322
	P value	0.5015	0.3255	0.1611	0.7982	0.2334
TLC	R square	0.3886	0.3198	0.2003	0.1388	0.1785
	P value	0.0099	0.0224	0.0822	0.1552	0.103
FVC	R square	0.1594	0.2036	0.272	0.05073	0.2064
	P value	0.1124	0.0691	0.0318	0.3847	0.0669

Table 3.7 – HU histogram data linear regression with lung function parameters.

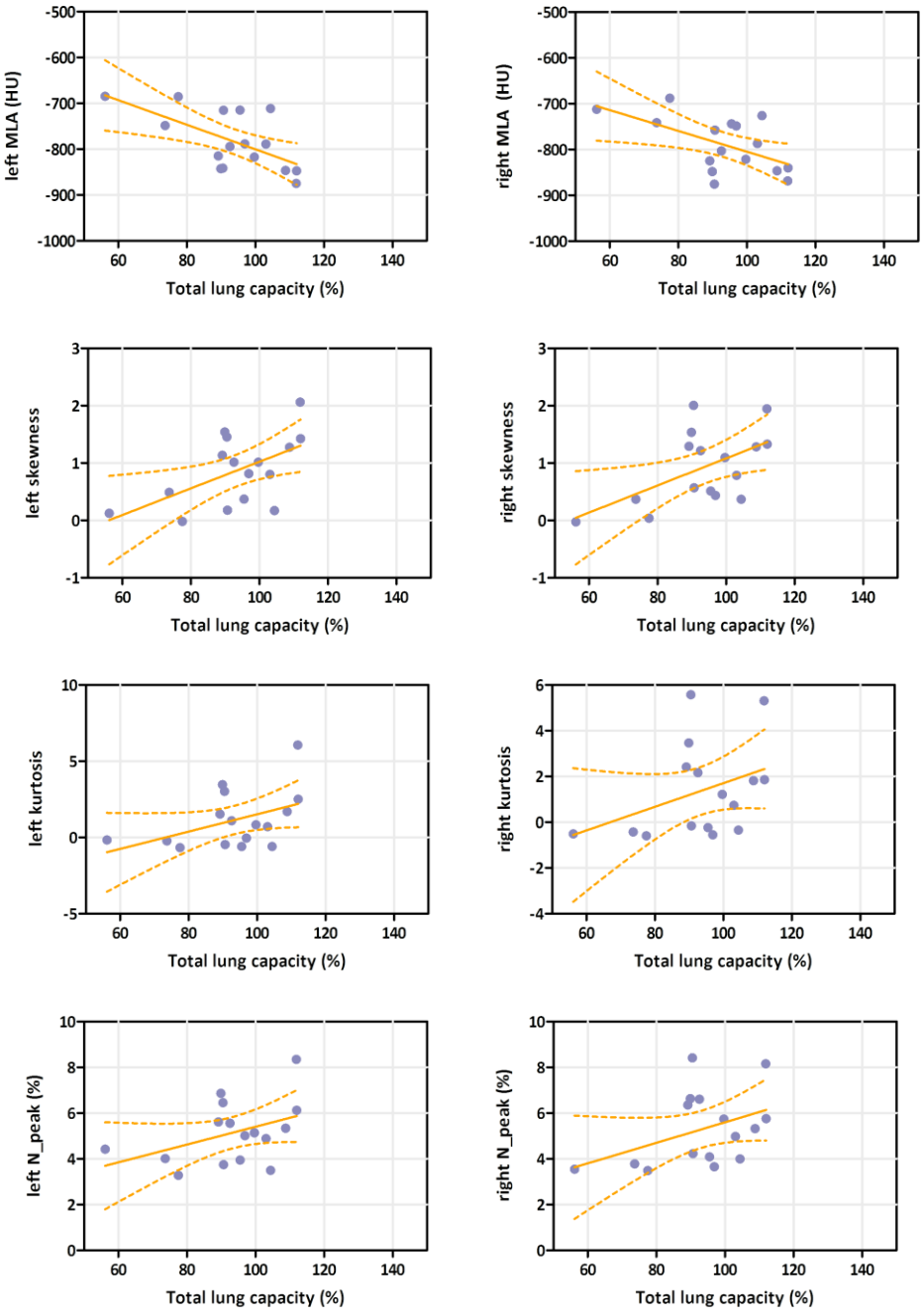

Figure 3.3 – Correlations of HU histogram data with TLC.

3.3.2 Correlation with image noise

We observed correlation of quantitative parameters with image noise. The results showed significant correlations of mean lung attenuation ρ=0.53, skewness ρ=-0.59, kurtosis ρ=-0.50, full-width at half-maximum ρ=0.56 and normalized peak height ρ=-0.54 to noise in air. The parameters of the right lung showed similar correlations. All these correlations were driven by 2 outlier values as shown on the individual graphs on Figure 3.4.

Color code:	Spearman r	≥ 0.50	≥ 0.60	≥ 0.70	≥ 0.75	≥ 0.80
	P value (two-tailed)	≤ 0.05	≤ 0.01	≤ 0.001	≤ 0.0001	

		leftMLA	left skewness	left kurtosis	left FWHM	left N_peak
Noise - Air	**Spearman r**	**0.5263**	**-0.585**	**-0.5023**	**0.5549**	**-0.5429**
	95% confidence interval	0,09521 to 0,7912	-0,8209 to -0,1785	-0,7786 to -0,06270	0,1350 to 0,8058	-0,7997 to -0,1181
	P value (two-tailed)	0.0171	0.0067	0.024	0.0111	0.0134
Noise - Fat	**Spearman r**	**0.3429**	**-0.4376**	**-0.2932**	**0.3564**	**-0.3504**
	95% confidence interval	-0,1314 to 0,6894	-0,7437 to 0,02028	-0,6593 to 0,1853	-0,1163 to 0,6974	-0,6939 to 0,1230
	P value (two-tailed)	0.1389	0.0537	0.2096	0.123	0.1299

Table 3.8 – HU histogram Spearman correlation with noise in air and noise in fat.

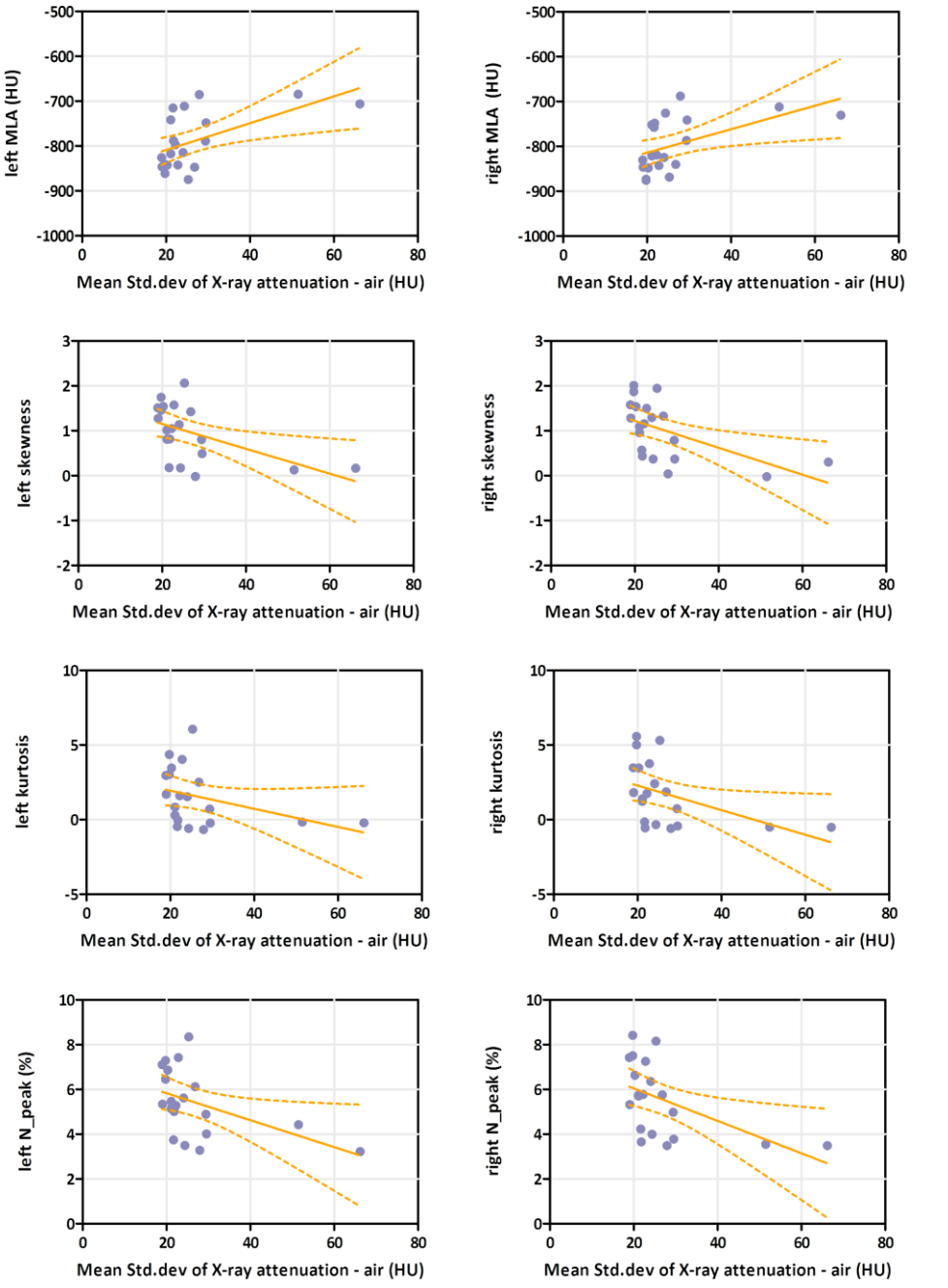

Figure 3.4 – Correlations of HU histogram data with image noise of air.

3.4 LungPBV histogram analysis

All of the parameters that have been computed in the HU Histogram data were analysed in LungPBV data, respectively. Table 3.9 shows the individual values of all patients for all 6 parameters.

	Mean		STD		Skew		Kurt		FWHH		N_Peak	
	Left	Right	Left	Right	Left	Right	Left	Right	Left	Right	Left	Right
Pilot01	10.180	9.857	16.891	16.494	-0.021	-0.038	-0.006	0.175	34.947	33.639	2.651	2.742
Pilot02	20.120	21.583	16.987	15.677	0.032	0.047	0.178	0.338	32.537	30.545	2.809	3.006
PIlot03	19.477	11.756	24.324	23.407	-0.151	0.057	-1.230	-1.227	41.973	39.819	2.131	2.254
Pilot04	18.500	18.639	26.521	22.069	-0.123	-0.094	-1.601	-0.776	39.783	38.851	2.183	2.293
Pilot05	24.055	24.176	13.855	12.188	-0.043	-0.005	1.056	0.954	26.269	25.700	3.441	3.636
Pilot06	21.217	21.541	18.712	16.599	-0.062	-0.011	-0.279	-0.177	32.576	29.156	2.747	3.106
Pilot07	21.218	20.981	12.314	11.462	-0.070	0.183	1.439	1.191	24.531	23.560	3.777	3.963
Pilot08	24.068	24.031	13.446	11.518	-0.011	-0.007	1.039	1.196	25.319	23.908	3.615	3.923
Pilot09	24.205	22.616	17.580	17.412	-0.232	-0.160	0.194	0.244	35.198	35.401	2.593	2.578
Pilot10	15.091	17.564	15.773	13.153	-0.010	-0.057	0.057	0.635	27.804	25.805	3.244	3.582
Pilot11	11.023	16.694	33.488	35.534	0.051	-0.020	-2.058	-2.298	57.844	54.975	1.589	1.650
Pilot12	14.891	13.048	15.369	11.753	-0.016	0.320	0.058	1.297	26.329	23.597	3.443	3.959
Pilot13	17.209	17.304	16.971	14.245	0.044	-0.055	-0.247	0.726	31.643	30.001	2.886	3.084
Pilot14	22.680	24.662	16.127	15.727	-0.373	-0.209	0.743	0.692	29.207	29.256	3.039	3.078
Pilot15	16.887	18.433	16.694	12.857	-0.082	0.019	-0.124	1.001	29.052	25.230	3.132	3.656
Pilot16	20.960	26.108	21.941	21.319	-0.111	-0.137	-0.956	-2.041	35.965	29.752	2.465	3.090
Pilot17	15.815	14.922	15.889	14.745	-0.011	0.045	0.203	0.549	30.870	30.265	2.971	3.055
Pilot18	21.662	17.079	18.616	15.956	-0.150	0.108	-0.472	0.054	37.934	37.559	2.468	2.555
Pilot20	16.344	17.331	15.691	12.443	0.140	0.143	-0.142	0.975	26.395	25.263	3.439	3.686
Pilot21	17.746	17.979	14.834	14.157	-0.121	-0.274	0.644	0.660	27.911	29.320	3.248	3.143
Pilot23	18.098	18.392	18.972	19.806	-0.016	-0.051	-0.168	-0.214	39.066	40.412	2.360	2.271
Pilot24	21.106	21.484	25.515	24.338	-0.194	-0.197	-0.986	-0.860	50.327	49.120	1.822	1.872
Pilot25	25.449	27.044	20.055	17.167	-0.301	-0.229	-0.223	0.231	38.146	34.360	2.375	2.661

Table 3.9 – LungPBV data of all histogram parameters previously described. STD = standard deviation, Skew = skewness, Kurt = kurtosis, FWHM = full-width at half-maximum, N_peak = normalized peak.

3.4.1 Correlations with LungPBV data

Color code:	Spearman r	≥ 0.50	≥ 0.60	≥ 0.70	≥ 0.75	≥ 0.80
	P value (two-tailed)	≤ 0.05	≤ 0.01	≤ 0.001	≤ 0.0001	

		left avgΔAtt	left skewness	left kurtosis	left FWHM	left N_peak
meanPAP	Spearman r	-0.3427	-0.07137	-0.2135	0.2815	-0.2504
	95% confidence interval	-0,6752 to 0,1055	-0,4888 to 0,3727	-0,5915 to 0,2413	-0,1720 to 0,6366	-0,6162 to 0,2043
	P value (two-tailed)	0.1185	0.7523	0.34	0.2044	0.2611
Body surface area - Dubois	Spearman r	-0.6081	0.3879	-0.2005	0.1304	-0.118
	95% confidence interval	-0,8240 to -0,2382	-0,05366 to 0,7026	-0,5825 to 0,2542	-0,3202 to 0,5329	-0,5238 to 0,3315
	P value (two-tailed)	0.0027	0.0744	0.3711	0.5629	0.6009
Age	Spearman r	0.2953	-0.371	-0.1146	0.1756	-0.1666
	95% confidence interval	-0,1574 to 0,6454	-0,6924 to 0,07337	-0,5213 to 0,3345	-0,2781 to 0,5652	-0,5589 to 0,2867
	P value (two-tailed)	0.1821	0.0892	0.6115	0.4344	0.4588
SVR	Spearman r	-0.04461	-0.1395	-0.02993	0.08413	-0.08526
	95% confidence interval	-0,4681 to 0,3956	-0,5395 to 0,3119	-0,4566 to 0,4079	-0,3616 to 0,4986	-0,4994 to 0,3606
	P value (two-tailed)	0.8437	0.5359	0.8948	0.7097	0.706
PVR	Spearman r	-0.1813	-0.205	-0.2885	0.4207	-0.3936
	95% confidence interval	-0,5692 to 0,2727	-0,5856 to 0,2497	-0,6411 to 0,1646	-0,01455 to 0,7219	-0,7059 to 0,04701
	P value (two-tailed)	0.4195	0.3602	0.1928	0.0512	0.07
AVDO2	Spearman r	-0.3586	-0.02089	-0.2547	0.4715	-0.4433
	95% confidence interval	-0,6849 to 0,08760	-0,4494 to 0,4154	-0,6190 to 0,1999	0,04889 to 0,7509	-0,7349 to -0,01322
	P value (two-tailed)	0.1013	0.9265	0.2527	0.0268	0.0388
art SO2	Spearman r	0.3129	0.06382	0.4936	-0.5332	0.5112
	95% confidence interval	-0,1384 to 0,6566	-0,3792 to 0,4831	0,07766 to 0,7632	-0,7848 to -0,1308	0,1009 to 0,7728
	P value (two-tailed)	0.1562	0.7778	0.0196	0.0106	0.015
ven SO2	Spearman r	0.223	0.1395	0.4568	-0.6431	0.6206
	95% confidence interval	-0,2319 to 0,5979	-0,3119 to 0,5395	0,03020 to 0,7426	-0,8416 to -0,2917	0,2570 to 0,8303
	P value (two-tailed)	0.3184	0.5359	0.0326	0.0012	0.0021

Table 3.10 – LungPBV Spearman correlations with RHC parameters, left lung (avgΔAtt = average change in attenuation).

Color code:	Spearman r	≥ 0.50	≥ 0.60	≥ 0.70	≥ 0.75	≥ 0.80
	P value (two-tailed)	≤ 0.05	≤ 0.01	≤ 0.001	≤ 0.0001	

		right avgΔAtt	right skewness	right kurtosis	right FWHM	right N_peak
meanPAP	Spearman r	-0.431	0.1393	-0.1042	0.3087	-0.3161
	95% confidence interval	-0,7279 to 0,001879	-0,3120 to 0,5394	-0,5136 to 0,3439	-0,1430 to 0,6539	-0,6586 to 0,1350
	P value (two-tailed)	0.0452	0.5363	0.6444	0.1622	0.1519
Body surface area - Dubois	Spearman r	-0.5234	0.001694	-0.09768	0.1553	-0.1316
	95% confidence interval	-0,7795 to -0,1175	-0,4312 to 0,4339	-0,5088 to 0,3497	-0,2973 to 0,5508	-0,5338 to 0,3192
	P value (two-tailed)	0.0124	0.994	0.6654	0.4902	0.5595
Age	Spearman r	0.1372	-0.09881	-0.09091	0.153	-0.17
	95% confidence interval	-0,3140 to 0,5379	-0,5096 to 0,3487	-0,5037 to 0,3556	-0,2994 to 0,5492	-0,5613 to 0,2834
	P value (two-tailed)	0.5426	0.6617	0.6874	0.4966	0.4495
SVR	Spearman r	-0.1395	0.2298	-0.02541	0.09543	-0.083
	95% confidence interval	-0,5395 to 0,3119	-0,2251 to 0,6025	-0,4530 to 0,4117	-0,3517 to 0,5071	-0,4977 to 0,3626
	P value (two-tailed)	0.5359	0.3035	0.9106	0.6727	0.7134
PVR	Spearman r	-0.3947	0.17	-0.2592	0.4658	-0.4715
	95% confidence interval	-0,7066 to 0,04568	-0,2834 to 0,5613	-0,6220 to 0,1953	0,04166 to 0,7477	-0,7509 to -0,04889
	P value (two-tailed)	0.0691	0.4495	0.2441	0.0289	0.0268
AVDO2	Spearman r	-0.6206	0.1022	-0.2897	0.5652	-0.5641
	95% confidence interval	-0,8303 to -0,2570	-0,3456 to 0,5121	-0,6418 to 0,1634	0,1756 to 0,8018	-0,8012 to -0,1740
	P value (two-tailed)	0.0021	0.6509	0.191	0.0061	0.0062
art SO2	Spearman r	0.3745	-0.04914	0.3395	-0.5168	0.5417
	95% confidence interval	-0,06933 to 0,6945	-0,4717 to 0,3918	-0,1091 to 0,6732	-0,7759 to -0,1085	0,1425 to 0,7893
	P value (two-tailed)	0.086	0.8281	0.1222	0.0138	0.0092
ven SO2	Spearman r	0.4783	0.04122	0.4647	-0.7357	0.7425
	95% confidence interval	0,05761 to 0,7547	-0,3985 to 0,4655	0,04023 to 0,7471	-0,8863 to -0,4447	0,4566 to 0,8894
	P value (two-tailed)	0.0244	0.8555	0.0293	< 0,0001	< 0,0001

Table 3.11 – LungPBV Spearman correlations with RHC parameters, right lung (avgΔAtt = average change in attenuation).

In the LungPBV dataset several correlations could be observed. Body surface area after Dubois (BSA) has shown ρ=-0.61 in Spearman correlation with average change in the attenuation. Furthermore, oxygen exchange parameters such as art SO_2 correlated with FWHM (ρ=-0.53) and normalized peak (ρ=0.51). A correlation of ven SO_2 with FWHM (ρ=-0.64) and normalized peak (ρ=0.62) was also observed. The parameters of the right lung showed similar correlations. The individual graphs for the correlations with artSO_2 are shown on Figure 3.5.

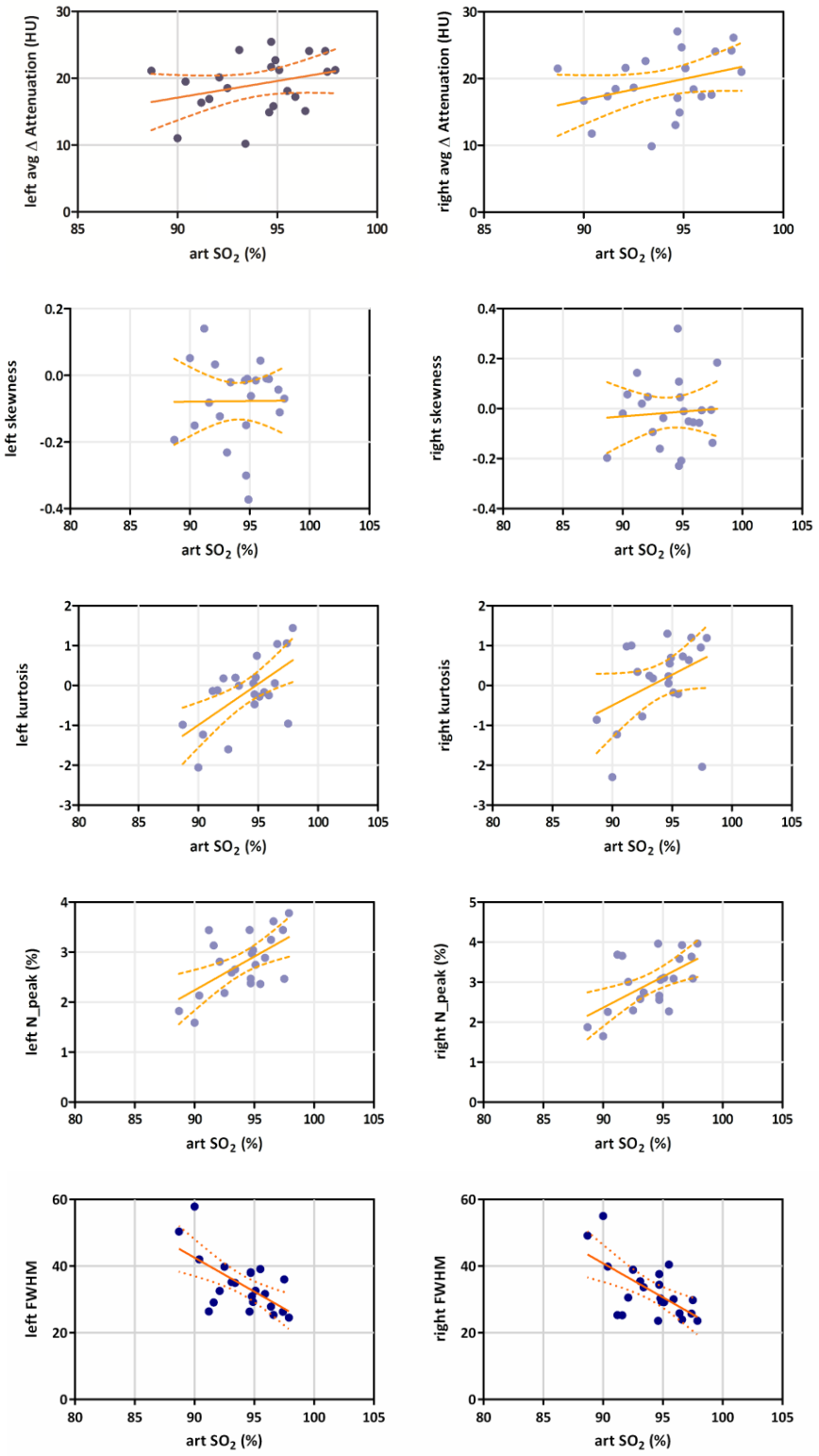

Figure 3.5 – Correlations of LungPBV data with art SO_2.

3.4.2 Correlations of LungPBV data with image noise

We observed correlation of LungPBV quantitative parameters with image noise. The results showed significant correlations of full-width at half-maximum ρ=0.78 and normalized peak height ρ=-0.79 to noise in air. Additionally, significant correlations of full-width at half-maximum ρ=0.54 and normalized peak ρ=-0.56 to noise in fat have been calculated. The parameters of the right lung showed similar correlations. These correlations were driven by 2 outliers as shown on Figure 3.4.

Color code:	Spearman r	≥ 0.50	≥ 0.60	≥ 0.70	≥ 0.75	≥ 0.80
	P value (two-tailed)	≤ 0.05	≤ 0.01	≤ 0.001	≤ 0.0001	

		left avgΔAtt	left skewness	left kurtosis	left FWHM	left N_peak
Noise - Air	**Spearman r**	**-0.1639**	**-0.1398**	**-0.4511**	**0.7774**	**-0.785**
	95% confidence interval	-0,5750 to 0,3132	-0,5583 to 0,3353	-0,7512 to 0,003420	0,5000 to 0,9102	-0,9134 to -0,5144
	P value (two-tailed)	0.4899	0.5565	0.0459	< 0,0001	< 0,0001
Noise - Fat	**Spearman r**	**-0.3128**	**0.1955**	**-0.4977**	**0.5429**	**-0.5639**
	95% confidence interval	-0,6713 to 0,1644	-0,2835 to 0,5964	-0,7762 to -0,05671	0,1181 to 0,7997	-0,8104 to -0,1479
	P value (two-tailed)	0.1794	0.4088	0.0255	0.0134	0.0096

Table 3.12 – Spearman correlations of LungPBV data with image noise.

3.4.3 Difference between quantitative parameters and WHO class

We observed differences of quantitative parameters of left and right lung between patients in different WHO class. Full-width at half-maximum and normalized peak height, reacting in opposite directions, showed a significant difference between WHO class II and III. WHO class I has only shown 2 patients in our pilot study, therefore this group could not be included in the statistical analysis.

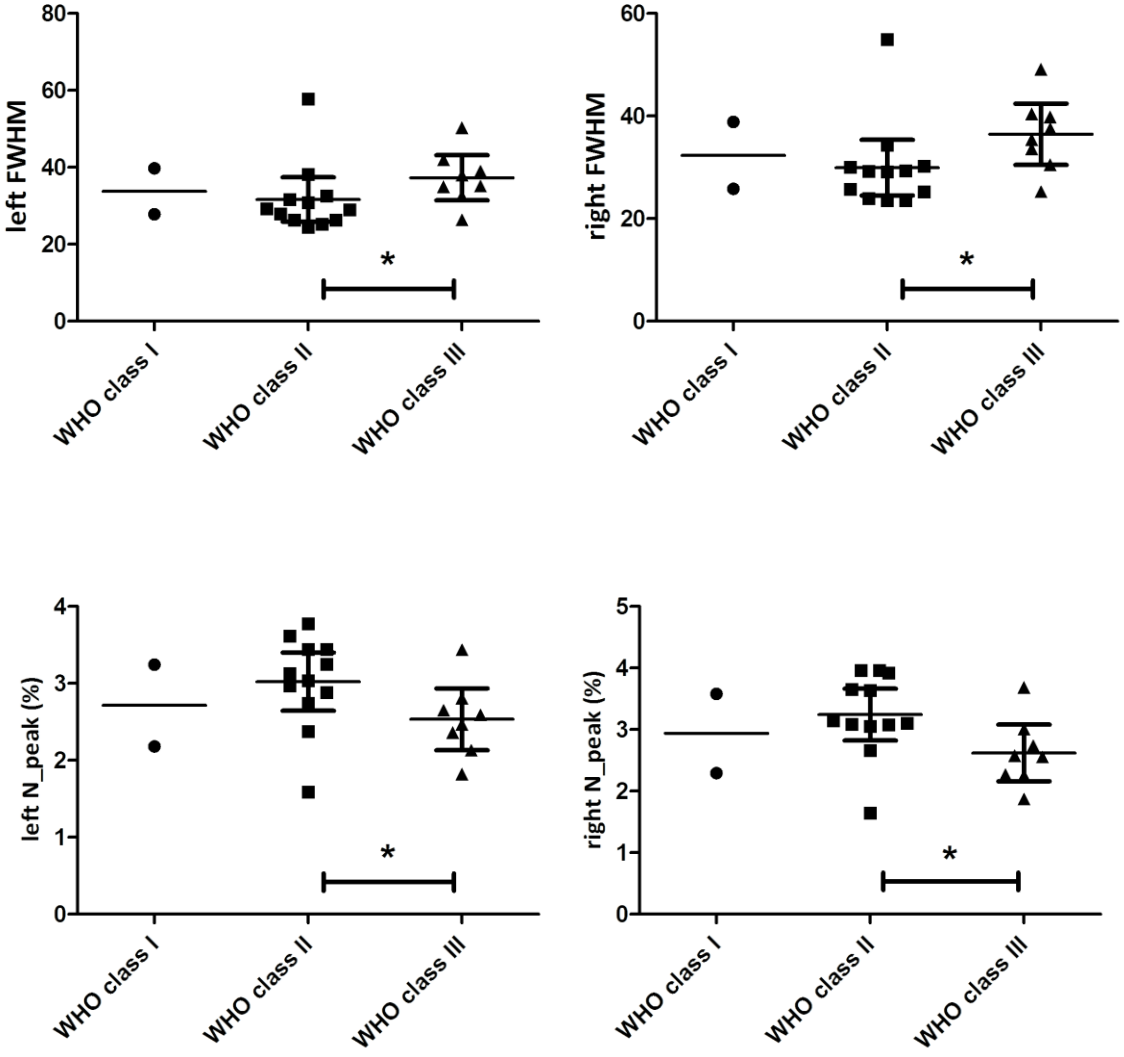

Figure 3.6 – WHO class, LungPBV FWHM and normalized peak height. Center lines indicate the mean, whiskers represent the standard deviation. (* $p < 0.05$)

3.4.4 Differentiation between PH and non-PH patients

The disease group analysis showed a significant difference of average difference in attenuation between patients having PH and those without PH. Our results provided similar values in the left and the right lung (Figure 3.7).

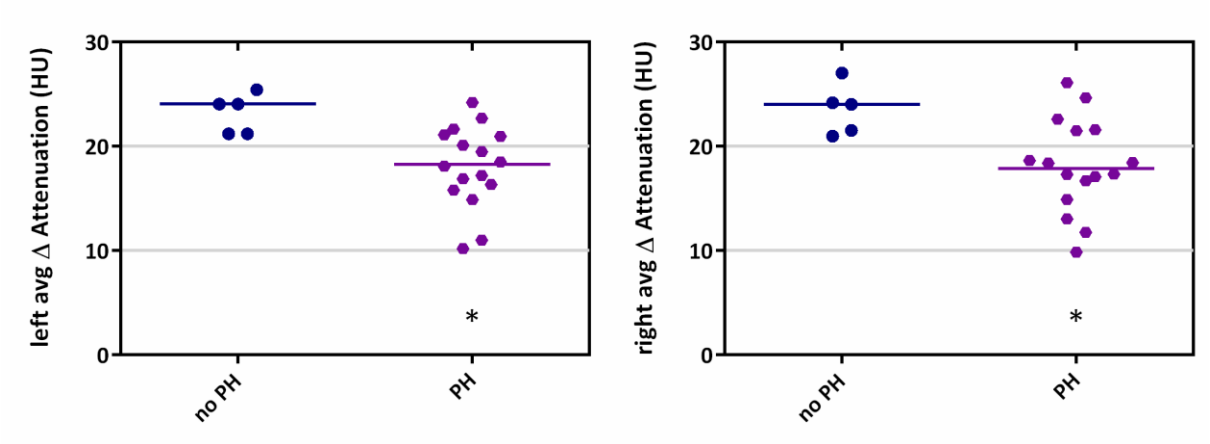

Figure 3.7 – Differentiation between PH and non-PH patients. avgΔAttenuation = average attenuation difference, PH = pulmonary hypertension. (* $p < 0.05$)

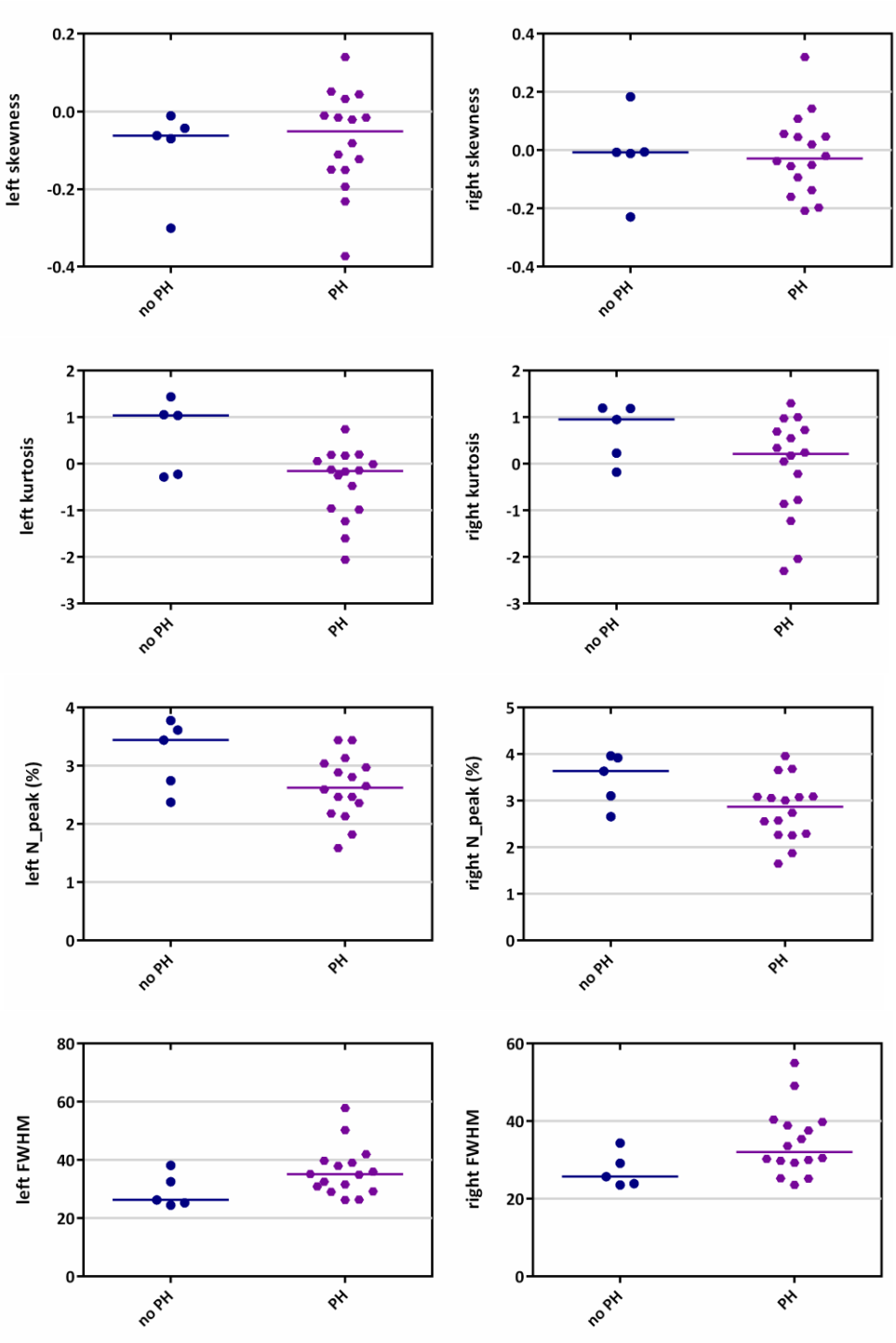

Figure 3.8 – Values of other histogram parameters.

Although not all parameters showed significant difference with PH diagnosis, a trend can be seen in the performed statistical analyses for increased FWHM and decreased N_peak in PH patients (Figure 3.8).

Chapter 4

Discussion

Firstly, the Hounsfield unit histogram data we calculated in our PH pilot study provide additive information in the diagnostic process of patients suffering from lung diseases. Although the clinical effectiveness of acquiring these values might seem limited, the implementation in daily routine could shorten the time to diagnosis. Quantitative data can give an indication for lung physiology changes based on any thoracic CT of a specific patient and therefore this information can prove valuable and must not be wasted.

Secondly, we performed in-depth analysis of lung perfused blood volume data. This technique requires dual-energy CT which is only available in specific centers. In our analysis we were able to distinguish between patients suffering from PH and those without PH. Preparing the way for non-invasive PH diagnosis, future work should focus on lung perfused blood volume data in a larger cohort to clarify the reliability of this method further.

Automatic lung segmentation is an important tool to get in-depth information of CT images. Especially in DECT images, the acquisition of an accurate lung segmentation can provide valuable disease specific data. However, the computational effort has to find its way in the diagnostic process and therefore has to fulfill several quality criteria. Our approach was to develop a fully automated algorithm without user intervention to minimise the effort needed to include it in daily routine. Furthermore, the computational time has to be in a meaningful range to allow automated lung segmentation and evaluation of quantitative parameters to take its place in diagnostics.

Quantitative analysis has not yet found its place as a novel biomarker in the detection of lung diseases such as pulmonary hypertension. Although recent work shows great potential in detailed quantitative analysis of HRCT in interstitial lung disease patients[3], more work has to be done to validate it as a diagnostic tool. In diffuse lung disease patients distinct histogram shapes has been shown for pathologic structures like ground-glass opacity, reticular opacity, honeycombing, emphysema and airspace consolidation[59]. It has also been shown that quantitative CT analysis bears valuable information about emphysema patterns in smokers[7].

Lung perfused blood volume is a technique provided by Siemens Somatom Definition Flash CT scanners used for representation of contrast agent induced changes in the lung parenchyma. One has to be cautious about possible misunderstanding of this data as they do not show direct perfusion, but rather a snapshot of the iodine distribution at a certain time point[63].

Our work provides a fully automated algorithm for lung segmentation and quantitative analysis of lung CT scans. The results shown have declared the connection to oxygen exchange parameters and the power to

differentiate patients in WHO class II from those in WHO class III. This can be of value in deciding further steps in the diagnostic process. Although oxygen exchange parameters can also be acquired by simple lung function testing, CT has a lot of indications in routine diagnostics and by using this method, can lead the physician to a different diagnostic tool. Most importantly our algorithm was able to differentiate patients having PH from those without PH.

As the awareness of pulmonary hypertension as a possible lung disease is quite low, the time needed to set this diagnosis is about 2 years[31]. Once our results are validated, the opportunity arises to establish a non-invasive diagnostic tool as additional marker for PH. Without the need of an additional, invasive procedure the usually routinely performed CT scan of a patient can be processed and an indication for the presence of pulmonary hypertension can be given. This can in another step lead to a decision of performing right-heart catheterization, gold standard for diagnosing PH, and the definite diagnosis of PH, together with an earlier onset of therapy.

4.1 Limitations

Several limitations of our study have to be mentioned. This has been a pilot study with n=25 patients, so our values have to be considered as a proof of concept. In order to validate these results, a prospective study has already achieved ethics approval and is currently running. Furthermore, no CT scans of healthy patients are available. Another limitation of our work is the threshold based parenchyma analysis. The HU of a CT scan can vary depending on tube voltages, body composition and expiration / inspiration level of a patient. Therefore there is still the need to develop an algorithm without taking fixed density values into consideration. Severe emphysematous areas or fibrotic changes of emphysema are hard to detect based on density values, because they can differ greatly from usual lung parenchyma density.

We consider that instead of the HU based histogram analysis one might include/focus on contrast agent based histogram for the determination of lung diseases, especially affecting the pulmonary oxygen exchange and/or perfusion parameters. Although lung perfused blood volume data suffers greatly from image noise, valuable information can be derived from it. There is still need to develop novel denoising techniques to reduce noise influence in these data.

4.2 Outlook

A different approach for lung parenchyma segmentation could be the subsequent dissection of the anatomic structures of the human thorax in the CT image by identifying structures like ribs, the heart or the spine. According to this set points and conditions that can be observed in every CT scan, it should be possible to calculate a lung parenchyma segmentation without using HU thresholds. In a second step it would increase the level of detail of this analysis by calculating lung lobe segmentation. More regional changes will be observable by selecting lung lobes as regions of interest. Additonally, whole lung parenchyma can be analysed by distributing the parenchyma to fixed volumes of interest. These volumes of interest can be analysed separately to increase the level of detail. Furthermore, an automatic trachea isolation algorithm would improve the accuracy of parenchyma detection.

4.3 Conclusion

We created a fully automated algorithm for detailed analysis of CT scans and computed the quantitative values of lung parenchyma in a pilot study. The results we observed show important information of disease parameters in our patient cohort. Our quantitative readouts of the volume histograms have shown correlations with lung function parameters for further clinical relevance. We have shown that lung perfused blood volume histogram normalized peak height and full-width at half-maximum can differentiate between PH and non-PH patients, bearing the potential of a basis for a diagnostic tool as thoracic dual-energy CT.

Chapter 5

Bibliography

[1] Badesch DB, Raskob GE, Elliott CG, Krichman AM, Farber HW, Frost AE, Barst RJ, Benza RL, Liou TG, Turner M, Giles S, Feldkircher K, Miller DP, and McGoon MD. Pulmonary arterial hypertension: baseline characteristics from the REVEAL Registry. Chest 2010;137(2):376–387.

[2] Barst RJ, McGoon M, Torbicki A et al. Diagnosis and differential assessment of pulmonary arterial hypertension. J Am Coll Cardiol 2004;43(12 Suppl S):40–47.

[3] Bartholmai B J, Raghunath S, Ronald A, Karwoski B A, Moua T, Rajagopalan S, Maldonado F, Decker P A, Robb R A. Quantitative Computed Tomography Imaging of Interstitial Lung Diseases. J Thorac Imaging 2013;28(5):298-307.

[4] Best AC, Lynch AM, Bozic CM, Miller D, Grunwald GK, Lynch DA: Radiology 2003;228:407-414.

[5] Bradlow W M, Gibbs J S R, Mohiaddin R H. Cardiovascular magnetic resonance in pulmonary hypertension. J Cardiovasc Magn Reson 2012;14:6.

[6] Bush A, Gray H, Denison D M. Diagnosis of pulmonary-hypertension from radiographic estimates of pulmonary arterial size. Thorax 1988;43:127-131.

[7] Castaldi P J, Estépar R S J, Mendoza C S, Hersh C P, Laird N, Crapo J D, Lynch D A, Silverman E K, Washko G R. Distinct Quantitative CT Emphysema Patterns are Associated with Physiology and Function in Smokers. Am J Respir Crit Care Med 2013;188:1083-1090.

[8] Chan A L, Juarez M M, Shelton D K et al. Novel computed tomographic chest metrics to detect pulmonary hypertension. BMC Med Imaging 2011;11:7.

[9] Chetty K G, Brown S E, Light R W. Identification of pulmonary-hypertension in chronic obstructive pulmonary-disease from routine chest radiographs. Am Rev Respir Dis 1982;126:338-341.

[10] Dournes G, Verdier D, Montaudon M, Bullier E, Rivière A, Dromer C, Picard F, Billes M A, Corneloup O, Laurent F, Lederlin M. Dual-energy CT perfusion and angiography in chronic thromboembolic pulmonary hypertension: diagnostic accuracy and concordance with radionuclide scintigraphy. Eur Radiol 2014;24(1):42-51.

[11] Fisher M R, Forfia P R, Chamera E et al. Accuracy of doppler echocardiography in the hemodynamic assessment of pulmonary hypertension. Am J Respir Crit Care Med 2009;179:615-621.

[12] Foris V, Kovacs G, Tscherner M, Olschewski A, Olschewski H. Biomarkers in Pulmonary Hypertension. What Do We Know? Chest 2013;144(1):274-283.

[13] Fortin J, Habenbacher W, Heller A et al. Non-invasive beat-to-beat cardiac output monitoring by an improved method of transthoracic bioimpedance measurement. Comput Biol Med 2006;36:1185-1203.

[14] Funk D J, Moretti E W, Gan T J. Minimally invasive cardiac output monitoring in the perioperative setting. Anesth Analg 2009;108:887-897.

[15] Gabrielsen A, Videbaek R, Schou M, Damgaard M, Kastrup J, Norsk P. Non-invasive measurement of cardiac output in heart failure patients using a new foreign gas rebreathing technique. Clin Sci 2002;102:247-252.

[16] Gaine S and Rubin L: Primary Pulmonary Hypertension. Lancet 1998;352:719-725.

[17] Galbán C J, Han M K, Boes J L, Chughtai K A, Meyer C R, Johnson T D, Galbán S, Rehemtulla A, Kazerooni E A, Martinez F J, Ross B D. Computed tomography-based biomarker provides unique signature for diagnosis of COPD phenotypes and disease progression.Nat Med. 2012;18:1711-5.

[18] Galie N, Hoeper M M, Humbert M et al. Guidelines for the diagnosis and treatment of pulmonary hypertension. Eur. Respir. J. 2009;34(6):1219–1263.

[19] Galie N, Manes A, Negro L et al. A meta-analysis of randomized controlled trials in pulmonary arterial hypertension. Eur Heart J 2009;30:394-403.

[20] Ganz W, Donoso R, Marcus H S, Forreste J S, Swan H J C. New technique for measurement of cardiac output by thermodilution in man. Am J Cardiol 1971;27:392-396.

[21] Ghofrani H A, Distler O, Gerhardt F, Gorenflo M, Grünig E, Haefeli W E, Held M, Hoeper M M, Kähler C M, Kaemmerer H, Klose H, Köllner V, Kopp B, Mebus S, Meyer A, Miera O, Pittrow D, Riemekasten G, Rosenkranz S, Schranz D, Voswinckel R, Olschewski H. Treatment of pulmonary arterial hypertension (PAH): Updated Recommendations of the Cologne Consensus Conference 2011. International Journal of Cardiology 2011;154S:S20-S33.

[22] Grosse C, Grosse A. CT findings in diseases associated with pulmonary hypertension: a current review. Radiographics 2010;30:1753-77.

[23] Gruenig E, Barner A, Bell M et al. Non-invasive diagnosis of pulmonary hypertension: ESC/ERS guidelines with updated commentary of the cologne consensus conference 2011. Int J Cardiol 2011;154:S3-S12.

[24] Hamada K, Nagai S, Tanaka S, Handa T, Shigematsu M, NAgao T, Mishima M, Kitaichi M, Izumi T. Significance of pulmonary arterial pressure and diffusion capacity of the lung as prognosticator in patients with idiopathic pulmonary fibrosis. Chest 2007;131:650-656.

[25] Hartley PG, Galvin JR, Hunninghake GW, Merchant JA, Yagla SJ, Speakman SB, Schwartz DA. High-resolution CT-derived measures of lung density are valid indexes of interstitial lung disease. J Appl Physiol 1994;76:271–277.

[26] Helderman F, Mauritz G, Andringa K E, Vonk-Noordegraaf A, Marcus J T. Early onset of retrograde flow in the main pulmonary artery is a characteristic of pulmonary arterial hypertension. Journal of Magnetic Resonance Imaging 2011;33:1362-1368.

[27] Hillis L D, Firth B G, Winniford M D. Analysis of factors affecting the variability of fick versus indicator dilution measurements of cardiac-output. Am J Cardiol 1985;56:764-768.

[28] Hoeper M, Maier R, Tongers J et al. Determination of cardiac output by the fick method, thermodilution, and acetylene rebreathing in pulmonary hypertension. Am J Respir Crit Care Med 1999;160:535-541.

[29] Hoeper M M, Lee S H, Voswinckel R et al. Complications of right heart catheterization procedures in patients with pulmonary hypertension in experienced centers. J Am Coll Cardiol 2006;48:2546-2552.

[30] Hoeper M M, Bogaard H J, Condliffe R, Frantz R, Khanna D, Kurzyna M, Langleben D, Manes A, Satoh T, Torres F, Wilkins M R, Badesh D B. Definitions and Diagnosis of Pulmonary Hypertension. J Am Coll Cardiol 2013;62:D42–50.

[31] Humbert M, Simonneau G. The Need for National Registries in Rare Diseases. AJRCCM 2006;173:1023-1030.

[32] International Commission on Radiological Protection ICRP. The 2007 recommendations of the international commission on radiological protection. ICRP publication 103. Ann ICRP 2007;37:1-332.

[33] Johnson T R C. Dual-Energy CT: General Principles. AJR 2012;199:3–8.

[34] Kessler R, Faller M, Fourgaut G, Mennecier B, Weitzenblum E. Predictive factors of hospitalization for acute exacerbation in a series of 64 patients with chronic obstructive pulmonary disease. Am J Respir Crit Care Med 1999;159:158-164.

[35] Kovacs G, Maier R, Aberer E, Brodmann M, Scheidl S, Tröster N, Hesse C, Salmhofer W, Graninger W, Gruenig E, Rubin LJ, Olschewski H. Borderline pulmonary arterial pressure is associated with decreased exercise capacity in scleroderma. Am J Respir Crit Care Med 2009;180:881-886.

[36] Kovacs G, Berghold A, Scheidl S, Olschewski H. Pulmonary arterial pressure during rest and exercise in healthy subjects: a systematic review. Eur Respir J 2009;34:888-894.

[37] Koyamaa H, Ohnob Y, Yamazakic Y, Nogamid M, Kusakae A, Murasec K, Sugimura K. Quantitatively assessed CT imaging measures of pulmonary interstitial pneumonia: Effects of reconstruction algorithms on histogram parameters. Eur J Radiol 2010;74:142-146.

[38] Lang I M, Plank C, Sadushi-Kolici R, Jakowitsch J, Klepetko W, Maurer G. Imaging in pulmonary hypertension. Jacc-Cardiovascular Imaging 2010;3:1287-1295.

[39] Matsuoka S, Washko GR, Yamashiro T, San Jose Estepar R, Diaz A, Silverman EK, Hoffman E, Fessler HE, Criner GJ, Marchetti N, et al.; National Emphysema Treatment Trial Research Group. Pulmonary hypertension and computed tomography measurement of small pulmonary vessels in severe emphysema. Am J Respir Crit Care Med 2010;181:218–225.

[40] Matthay R A, Schwarz M I, Ellis J H et al. Pulmonary-artery hypertension in chronic obstructive pulmonary-disease - determination by chest radiography. Invest Radiol 1981;16:95-100.

[41] McLaughlin V. Managing pulmonary arterial hypertension and optimizing treatment options: prognosis of pulmonary artery hypertension. Am J Cardiol 2013;111(8):10C-15C.

[42] McLure L E R, Brown A, Lee W N, Curch A C, Peacock A J, Johnson M K. Non-invasive stroke volume measurement by cardiac magnetic resonance imaging and inert gas rebreathing in pulmonary hypertension. Clinical Physiology and Functional Imaging 2011;31:221-226.

[43] Meinel F G, Graef A, Thierfelder K M, Armbruster M, Schild C, Neurohr C, Reiser M F, Johnson T R C. Automated Quantification of Pulmonary Perfused Blood Volume by Dual-Energy CTPA in Chronic Thromboembolic Pulmonary Hypertension. Eur J Radiol 2014;186(2):151-6.

[44] Meyer S, Todd D, Wright I, Gortner L, Reynolds G. Review article: Non-invasive assessment of cardiac output with portable continuous-wave doppler ultrasound. Emergency Medicine Australasia 2008;20:201-208.

[45] Okajima Y, Ohno Y, Washko G R, Hatabu H. Assessment of pulmonary hypertension: What CT and MRI can provide. Acad Radiol 2011;18:437-453.

[46] Olschewski H, Hoeper MM, Borst MM, Ewert R, Grünig R, Kleber FX, Kopp B, Opitz C, Reichenberger F, Schmeisser A, Schranz D, Schulze-Neick I, Wilkens H, Winkler J, Worth H. Diagnosis and Therapy of Chronic Pulmonary Hypertension. Pneumologie 2006;60:749-771.

[47] Petter H, Erik A, Bjorn E, Goran R. Measurement of cardiac output with non-invasive aesculon (R) impedance versus thermodilution. Clinical Physiology and Functional Imaging 2011;31:39-47.

[48] Pienn M, Kovacs G, Tscherner M, Johnson T R, Kullnig P, Stollberger R, Olschewski A, Olschewski H, Bálint Z. Determination of cardiac output with dynamic contrast-enhanced computed tomography. Int J Cardiovasc Imaging 2013;29(8):1871-8.

[49] Pienn M, Kovacs G, Tscherner M, Avian A, Johnson T R, Kullnig P, Stollberger R, Olschewski A, Olschewski H, Bálint Z. Non-invasive determination of pulmonary hypertension with dynamic contrast-enhanced computed tomography. Eur Radiol 2014;24(3):668-76.

[50] Porhomayon J, El-Solh A, Papadakos P, Nader N D. Cardiac ouput monitoring devices: An analytic review. Internal and Emergency Medicine 2012;7:163-171.

[51] Reiter G, Reiter U, Kovacs G et al. Magnetic resonance-derived 3-dimensional blood flow patterns in the main pulmonary artery as a marker of pulmonary hypertension and a measure of elevated mean pulmonary arterial pressure. Circulation-Cardiovascular Imaging 2008;1:23-30.

[52] Remy-Jardin M, Faivre J-B, Pontana F, Molinari F, Tacelli N, Remy J. Thoracic Applications of Dual Energy. Semin Respir Crit Care Med 2014;35:64-73.

[53] Sanz J, Kuschnir P, Rius T et al. Pulmonary arterial hypertension: Noninvasive detection with phase-contrast MR imaging. Radiology 2007;243:70-79.

[54] Simonneau G, Gatzoulis M A, Adatia I, Celermajer D, Denton C, Ghofrani A, Gomez Sanchez M A, Krishna Kumar R, Landzberg M, Machado R F, Olschewski H, Robbins I M, Souza R. J Am Coll Cardiol. 2013;62:34-41.

[55] Sitbon O, Humbert M, Nunes H, Parent F, Garcia G, Hervé P, Rainisio M, Simonneau G. Long-term intravenous epoprostenol infusion in primary pulmonary hypertension: prognostic factors and survival. J Am Coll Cardiol 2002;40:780-788.

[56] Stauber R E, Olschewski H. Portopulmonary hypertension: short review. European Journal of Gastroenterology & Hepatology 2010;22:385-390.

[57] Stengel D, Bhandari M, Hanson B: Statistik und Aufbereitung klinischer Daten. 2010.

[58] Stevens GR, Fida N, Javier S, et al. Computed tomography and cardiac magnetic resonance imaging in pulmonary hypertension. Prog Cardiovasc Dis 2012;55:161-171.

[59] Sumikawa H, Johkoh T, Yamamoto S, Yanagawa M, Inoue A, Honda O, Yoshida S, Tomiyama N, Nakamura H. Computed Tomography Values Calculation and Volume Histogram Analysis for Various Computed Tomographic Patterns of Diffuse Lung Diseases. J Comput Assist Tomogr 2009;33(5):731-8.

[60] Tolle J J, Waxman A B, Van Horn T L, Pappagianopoulos P P, Systrom D M. Exercise-induced pulmonary arterial hypertension. Circulation 2008;118:2183-2189.

[61] Weitzenblum E, Hirth C, Ducolone A, Mirhom R, Rasaholinjanahary J, Ehrhart M. Prognostic value of pulmonary artery pressure in chronic obstructive pulmonary disease. Thorax 1981;36:752-758.

[62] Wong D, Tremper K, Stemmer E et al. Noninvasive cardiac-output - simultaneous comparison of 2 different methods with thermodilution. Anesthesiology 1990;72:784-792.

[63] https://www.healthcare.siemens.de/computed-tomography/options-upgrades/clinical-applications/syngo-de-lung-pbv. 21.04.2014.

[64] http://what-when-how.com/introduction-to-video-and-image-processing/morphology-introduction-to-video-and-image-processing-part-2/. 16.03.2014.

[65] http://www.scilogs.com/mmmbitesizescience/converting-weeds-into-flowers-artificial-stem-cells-create-a-blood-supply-for-bioengineered-organs/. 19.09.2013.